Geochemical Transactions

RESEARCH

Open Access

Water quality assessment of Upper Ganga and Yamuna river systems during COVID-19 pandemic-induced lockdown: imprints of river rejuvenation

Sameer K. Tiwari[1*], Jairam Singh Yadav[1], Kalachand Sain[1], Santosh K. Rai[1], Aditya Kharya[1], Vinit Kumar[1] and Pratap Chandra Sethy[1]

Abstract

Clean river water is an essential and life-sustaining asset for all living organisms. The upper Ganga and Yamuna river system has shown signs of rejuvenation and tremendous improvement in the water quality following the nationwide lockdown due to the coronavirus pandemic. All the industrial and commercial activity was shut down, and there was negligible wastewater discharge from the industries. This article addresses the water quality assessment from the study area, which is based on the original data of physical parameters, major and trace elements, and stable isotopes (hydrogen and oxygen) systematics during the nationwide lockdown. The impact of the lockdown could be seen in terms of an increase in dissolved oxygen (DO). Water samples were collected from the Upper Ganga and Yamuna river basins (Alaknanda, Bhagirathi, and Tons rivers) during an eight-week lockdown in Uttarakhand, India. We discussed the signs of rejuvenation of riverine based on physical parameters, major ions, trace elements, isotopic ratios, and water pollution index (WPI). Results reveal that the water quality of the entire upper basins of the Ganga has significantly improved by 93%, reflecting the signs of self-rejuvenation of the rivers. Multivariate analysis suggests a negative factor loading for an anthropogenic element (NO_3^-), implying that they contribute little to the river water during the lockdown. Further, bicarbonate (HCO_3^-) is a dominant element in both river basins. The geochemical facies are mainly characterized by the (Ca^{2+} : Mg^{2+} : HCO_3^-) type of water, suggesting that silicate rock weathering dominates with little influence from carbonate weathering in the area. The positive factor loadings of some cations, likeHCO_3^-,Ca^{2+}, and Mg^{2+} reflect their strong association with the source of origin in the lockdown phases. Stable isotopic reveals that the glaciated region contributed the most to the river basin, as evidenced by the low d-excess in riverine water compared to anthropogenic contributions. Rivers can self-rejuvenate if issues of human influence and anthropogenic activities are adequately resolved and underline our responsibility for purifying the ecosystem. We observed that this improvement in the river water quality will take a shorter time, and quality will deteriorate again when commercial and industrial activity resumes.

Keywords COVID-19, Lockdown, Riverine system, Major ions, Stable isotopes, Water quality

*Correspondence:
Sameer K. Tiwari
stiwariisr@gmail.com; sameer@wihg.res.in
[1] Wadia Institute of Himalayan Geology, 33 GMS Road, Dehradun 248001, Uttarakhand, India

Introduction

The COVID-19 pandemic originated in December 2019 in Wuhan, China, and spread quickly globally [18, 91, 128]. Nationwide lockdown (phase-1) was imposed in India on March 25th, 2020, and extended up to April 14th, 2020, to break the chain of the COVID-19 pandemic and extended until May 17th, 2020 (Phase-2). The World Health Organization apprised that there were five lakh confirmed cases, while more than three lakhs lost their lives across 216 countries due to COVID-19 [120]. Unfortunately, the deadly pandemic (COVID-19) continues in 2021, and from March 2021, more than 50,000 cases have been reported in India every day and found maximum in May. Presently, the number of COVID-19 deaths reported to WHO (cumulative total) worldwide to date is 7.1 million, and confirmed cases are 776 million and increasing (https://data.who.int/).

In India, the environmental conditions were temporarily improved because of the reduced pollution load during the nationwide lockdown. The aerosol concentrations were measured at a 20-year low based on the satellite data on optical depth measurements over the Indo-Gangetic Plains (IGP). It was possible due to the restrictions imposed on industries, air, rail, road transport, etc. [70]. The Ganga River Basin (GRB) is the largest source of fresh water for the most densely populated region globally [69, 79]. However, the effect of the COVID-19 lockdown on the water quality of the River Ganga was debatable. As stated by the Central Pollution Control Board (CPCB) of India, the Ganga River (2601 km length) has been exposed to high pollution over the last few decades [72]. Although the Ganga River is an essential life-supporting component of the rapidly growing population of India, human health is endangered due to its water pollution level. Earlier, the river water was polluted by various human activities such as industrialization, urbanization, agricultural practices, and overexploitation [8]. It has been stated that the pollution level of the riverine system has dropped during the lockdown period [39], as the primary pollution sources (e.g., industries, tourism activities, pilgrimage, hotels and lodges, shops) of the Ganga River were closed. However, the domestic discharges from the household continued during the lockdown period [34].

Garrels and Mackenzie [35] raised a fundamental question about the derivation of major ions in river water from its sources, which was later successfully addressed globally by several studies [6, 10, 13, 16, 25, 27, 30–32, 75, 89, 98, 103, 108]. Riverine water quality across the globe has degraded due to unplanned urbanization, human intervention, population growth, and anthropogenic activity [7, 39, 44, 100, 103]. Monitoring the water quality of major rivers is essential as these provide water and food security to about 3 billion people around the globe [7].

Water quality monitoring to quantify the impact of rapid population and industrial waste in the riverine system in India has gained momentum in the last two decades [29, 54, 103]. The Ganga–Brahmaputra basin spreads over one million km^2 and ranks among the most densely populated regions, with a population density of > 300 people/km^2, and is home to over 0.6 billion people in India [80]. India has minimal geochemical and isotopic data on rivers related to water quality assessment, including the Ganga River and its tributaries, which stated how the riverine water quality has deteriorated over time [11, 60, 93, 103, 115].

The print and electronic media stated that the overall pollution in the Ganga river is down by up to 50% due to the imposition of lockdown [41, 76, 77, 109, 110]. That has made the Ganga water potable by filtering without further treatment [5, 45]). Dissolved Oxygen (DO), Biochemical oxygen demand (BOD), and other physical parameters levels were improved during the lockdown, making the water drinking and bathing purposes [26]. These results were based on some observations (satellite data and physical parameters). Still, no geochemical and isotopic data is available to assess riverine water quality based on major ions, trace metals, and environmental isotopes. Based on isotope and geochemical studies, we report the scientific evidence for improved water quality in the Upper Ganga and Upper Yamuna River systems (UGRS and UYRS). If the concentrations of physical parameters, trace elements, and major ions surpass the permissible limit, they may harm humankind and livelihood [12, 19, 73]. Thus, measuring these parameters is essential to understand the water quality of any water masses.

The quality of water from a particular source (e.g., riverine/lake/groundwater) can assessed by its physiochemical and biological parameters. A method known as the Water Quality Index (WQI) is classified by giving unequal weightage based on its importance to riverine water quality, but there are certain limitations to this method [64, 85, 116]. Therefore, to avoid complications and reduce the errors and sensitivity of water indexing, we adopted a new, improved concept called Water Pollution Index for the present study [42].

Since the analysis of a dataset of variable magnitude and density is challenging, multivariate statistical techniques, namely Principal Component Analysis (PCA), can be applied to assess the water quality [3, 37, 43, 126]. This method requires significant sources of ions in river basins [58, 61, 114, 121]. The PCA provides a simple solution to the problems, whereas the conventional method fails to interpret the data. Hence, multi-dimensional

matrices and measurements have been preferred over new approaches to conventional ones [56].

Multivariate analysis, such as the Principal Component Analysis (PCA) and Hierarchical Cluster Analysis (HCA), are essential statistical methods to assess the water quality that includes the major sources of ions in river basins [63, 78, 121]. Analyzing the resulting dataset of variable magnitude and density is difficult. Therefore, multivariate statistical techniques are applied worldwide [3, 37, 43, 59, 114, 126]. Further, the hydrogeochemical evolution of the river water basin can be identified through the interpretation of PC loadings [4, 68].

Hydro-geochemical processes operating in the river basin are characterized by negative loadings on specific variables in terms of principal components. For example, low-negative loading on pH for Ca and Mg corresponds to high positive loading. The inverse correlation is generally seen between two negative loadings on pH and derivatives of carbonate ions [62].

In extensive hydrological studies, the stable isotopes of oxygen and hydrogen have been used as conservative tracers [38]. Numerous interpretations of hydrological processes occurring both on the surface and within aquifers have been influenced by stable water isotopes and solutes [50, 127]. For instance, they have been applied to identify water sources, flow patterns, and water mixing in various bodies of water [2, 38, 52]. In extensive hydrological studies, the stable isotopes of oxygen and hydrogen have been used as conservative tracers [38]. Numerous interpretations of hydrological processes occurring both on the surface and within aquifers have been influenced by stable water isotopes and solutes [50, 127]. For instance, they have been applied to identify water sources, flow patterns, and water mixing in various bodies of water [2, 38, 52].

We have calculated the WPI and compared the results with those carried out earlier in the same basin [16, 97] to quantify the improvement in water quality throughout the lockdown time. The rivers carry the products produced by continental weathering to the oceans and play a vital role in the evolution of global sea water [31, 32]. The carbonate and silicate weathering processes are also carried out at alterable scales, resulting in heterogeneity in river water composition [16].

This article addresses the water quality assessment for the first time during the COVID-19 pandemic-induced lockdown based on the original data of physical parameters, major and trace elements, and stable isotopes (hydrogen and oxygen) systematics. We discussed the signs of rejuvenation of riverine water against the average geochemical composition, isotopic ratios, and water pollution index (WPI) of the earlier studies of this region.

The main objectives of this study are: (1) To analyze the impact of the lockdown on the water quality of the Ganga River and its major tributary, Yamuna, in Uttarakhand; (2) To discuss issues and challenges to understand the magnitude of contamination and source relations and potential ways to improve the water quality using PCA and HCA; (3) To provide the essential implications for future restoration strategies on river rejuvenation; and (4) To generate the baseline data for future study on the water quality assessment from the Ganga river system.

Study area

General description

Present work is carried out in the headwaters of the Ganga and Yamuna river systems (UGRS) in the Himalayan region of Uttarakhand. The study area in the UGRS lies between latitudes 78°00′ N-78°50′ N and longitudes 29°50′-30°20′E, which extends from about 10 km upstream of the Alaknanda River at Mulya and 25 km upstream of the Bhagirathi river (at Koteshwar Dam) to up to Devprayag, where these two rivers join to become the Ganga river and further up to Haridwar city. Similarly, the area in the upper reaches of the Upper Yamuna River System (UYRS) lies between latitudes 77°50′N-78°10′N and longitudes 30°10′-30°30′E, which extends from upstream of Yamuna River at Barkot till down to Dakpather, Vikas Nagar. The sample locations are given in (Fig. 1, Tables 1, and 2). The Upper Ganga River system (UGRS) comprises two glacier-fed rivers, namely the Bhagirathi River basin (catchment area: 7.8×103 km^2) and the Alaknanda River basin (catchment area: 11.8×103 km^2) [14, 105]. Bhagirathi River originates from the Gangotri glacier at an elevation of 3900 m a.m.s.l. [107] joins with the Alaknanda River, which has its source from Satopanth and Bhagirath Kharak glacier system, at an elevation of 3641 m a.m.s.l. [95]. At Devprayag, from where they flow as the mighty river Ganga.

The Yamuna River originates from Saptrishi Kund near Bander Punchh peak (latitude 31.01°N, longitude 78.46°E) in the Mussoorie range of the lower Himalaya [60]. The Yamuna and its major tributaries (the Tons, the Giri, the Aglar, the Bata, and the Asan) form the Himalaya Yamuna River System (YRS). The YRS is fed mainly by the Indian summer monsoon and has its maximum discharge during July–September, the monsoon season. Its catchment receives about 80% of its annual rainfall during these months [21]. Further, the Yamuna and the Tons receive water from glacier melt, a major contributor to the discharge from April to June during the study period. The Yamuna joins the Ganga at Allahabad in the plains.

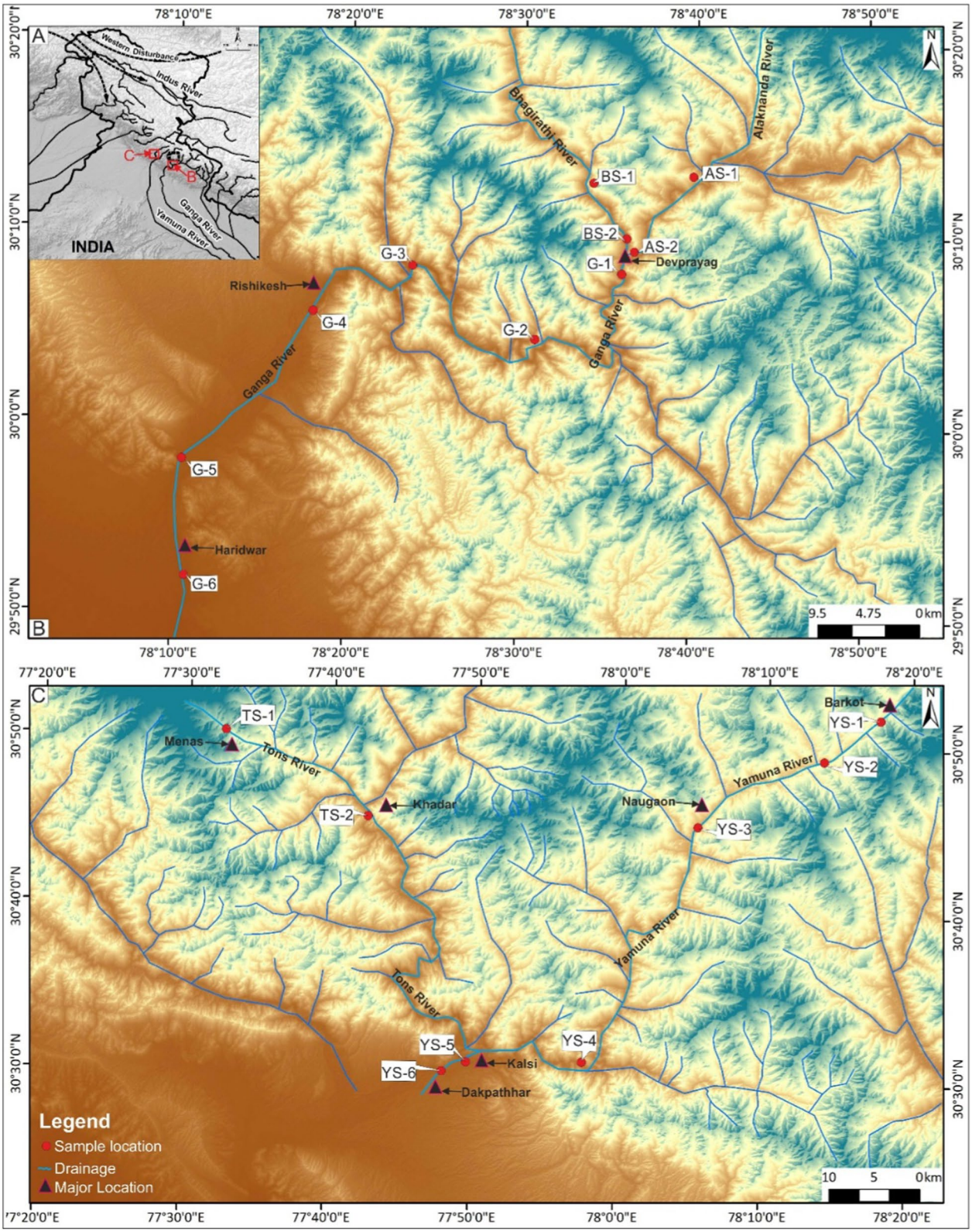

Fig. 1 **A** Inset image of India, pictorial diagram. **B** and **C** showing the studied catchments and the sample locations in the Upper Ganga River System and Upper Yamuna River System

Table 1 Geographical distribution of the samples (Upper Ganga River System)

	S. No.	Period of lockdown	Date	Sample ID	Sample name	Description	Latitude (N)	Longitude (E)	Elevation (m asl)
Upper Ganga river system	1	May, 2020 (Lockdown (Phase-1)	04/05/2020	AS-1	Alaknanda	Upstream 10 km from Devprayag, Near baba Ramdev Grukul	30° 12′ 20″	78° 38′ 41″	475
	2		04/05/2020	BS-1	Bhagirathi	Upstream 25 km from Devprayag at Jakholi (Koteswar Mahadev)	30° 14′ 55″	78° 31′ 36″	600
	3		04/05/2020	BS-2	Bhagirathi	before the confluence of the Alaknanda and Bhagirathi rivers at devprayag	30° 09′ 07″	78° 35′ 58″	456
	4		04/05/2020	AS-2	Alaknanda	before the confluence of the Alaknanda and Bhagirathi rivers at devprayag	30° 08′ 40″	78° 36′ 03″	443
	5		04/05/2020	G-1	Ganga	after the confluence of Alaknanda and Bhagirathi at Ramkund, Devprayag	30° 08′ 22″	78° 35′ 49″	490
	6		05/05/2020	G-2	Ganga	At Kodiyala	30° 04′ 23″	78° 30′ 05″	409
	7		05/05/2020	G-3	Ganga	at 1 km upstream from Shivpuri	30° 08′ 19″	78° 23′ 57″	371
	8		05/05/2020	G-4	Ganga	upstream of Virbhadra barrage	3°0 04 27″	78° 17′ 26″	329
	9		05/05/2020	G-5	Ganga	at VIP Ghat, Har ki Pauri, in front of Bhimgoda Barrage	29° 57′ 27″	78° 10′ 39″	272
	10		05/05/2020	G-6	Ganga	at Gajiwala 10 km downstream of Haridwar	29° 53′ 06″	78° 10′ 27″	249
	1	June, 2020 (Lockdown (Phase-2)	12/06/2020	AS-1	Alaknanda	Upstream 10 km from Devprayag, Near baba Ramdev Grukul	30° 12′ 20″	78° 38′ 41″	475
	2		12/06/2020	BS-1	Bhagirathi	Upstream 25 km from Devprayag at Jakholi (Koteswar Mahadev)	30° 14′ 55″	78° 31′ 36″	600
	3		12/06/2020	BS-2	Bhagirathi	before the confluence of the Alaknanda and Bhagirathi rivers at devprayag	30° 09′ 07″	78° 35′ 58″	456
	4		12/06/2020	AS-2	Alaknanda	before the confluence of Alaknanda and Bhagirathi at devprayag	30° 08′ 40″	78° 36′ 03″	443
	5		12/06/2020	G-1	Ganga	after the confluence of the Alaknanda and Bhagirathi rivers at Ramkund, Devprayag	30° 08′ 22″	78° 35′ 49″	490
	6		11/06/2020	G-2	Ganga	At Kodiyala	30° 04′ 23″	78° 30′ 05″	409
	7		11/06/2020	G-3	Ganga	01 km upstream from Shivpuri	30° 08′ 19″	78° 23′ 57″	371
	8		11/06/2020	G-4	Ganga	upstream of Virbhadra barrage	30° 04′ 27″	78° 17′ 26″	329
	9		11/06/2020	G-5	Ganga	at VIP Ghat, Har ki Pauri, in front of Bhimgoda Barrage	29° 57′ 27″	78° 10′ 39″	272
	10		11/06/2020	G-6	Ganga	at Gajiwala 10km downstream of Haridwar	29° 53′ 06″	78° 10′ 27″	249

Table 2 Geographical distribution of the samples (Upper Yamuna River System)

	S. No.	Period of lockdown	Date	Sample ID	Description	Latitude (N)	Longitude (E)	Elevation (m asl)
Upper Yamuna river system	1	May, 2020 (Lockdown Phase-1)	05/05/2020	YS-1	Yamuna River at Barkot	30° 32′ 16″	78° 11′ 57″	1153
	2		05/05/2020	YS-2	The Yamuna at 20 km upstream of Damta village	30° 45′ 09″	78° 05′ 35″	1099
	3		05/05/2020	YS-3	Yamuna 5 km Upstream of Juddo Village	30° 31′ 17″	77° 57′ 14″	848
	4		04/05/2020	TS-1	Tons river at Menas Village	30° 45′ 38″	77° 42′ 21″	732
	5		04/05/2020	TS-2	Tons river at Khadar before the confluence with Yamuna river	30° 48′ 54″	77° 32′ 16″	470
	6		05/05/2020	YS-4	Yamuna river at Dakpathar after the confluence with Tons	30° 30′ 39"	77° 49′ 41″	370
	1	June, 2020 (Lockdown Phase-2)	13/06/2020	YS-1	At Badkot	30° 32′ 16″	78° 11′ 57″	1153
	2		14/06/2020	YS-2	At Naogaon	30° 47′ 10″	78° 08′ 00″	1120
	3		14/06/2020	YS-3	20 km upstream of Damta village	30° 45′ 09″	78° 05′ 35″	1099
	4		14/06/2020	YS-4	5 km upstream of Juddo village	30° 31′ 17″	77° 57′ 14″	848
	5		13/06/2020	TS-1	Tons river at Menas Village	30° 45′ 38″	77° 42′ 21″	732
	6		13/06/2020	TS-2	Tons at Khadar, before the confluence with the Yamuna river	30° 48′ 54″	77° 32′ 16″	470
	7		13/06/2020	YS-5	Yamuna River Kalsi before the confluence with Tons River	30° 30′ 42″	77° 49′ 54"	475
	8		14/06/2020	YS-6	At Dak Patthar aft. Confluence with Tons River	30° 30′ 39″	77° 49′ 41"	370

Geological setup

The Upper Ganga Rivers system and its tributaries flow mainly through the Higher Himalayan crystalline (HHC) and Lesser Himalayan sedimentary (LHS) lithology. However, some of their tributaries originate in the Tethyan sediments. HHC in the study area consists of high-grade gneisses, metabasite, quartzite, schist, and granite, with a trace amount of carbonate and calc-silicate rocks [81, 123]. After originating from the HHC, the Bhagirathi River drains through a deep gorge at Gangotri, crosses the Bhagirathi leucogranite, and travels to the village of Bhatwari where it crosses the Vaikrita Thrust at Gangnani [106]. According to [101], the Vaikrita Thrust marks the upper boundary of the Main Central Thrust (MCT), which is also defined as a zone of high ductile strain bounded by an upper thrust, MCT-II (Vaikrita Thrust) and a lower thrust, MCT-I (Munsiari Thrust).

Alaknanda River originates about 13 km upstream from the temple at Badrinath in the HHC rocks in the footwall of the South Tibetan Detachment (STD) Fault. After originating from the glacier, the river drains through a narrow and deep gorge of high-grade HHC rocks—grading from garnet-biotite-muscovite-schists from the base of the MCT to sillimanite-kyanite schists, psammitic gneiss, migmatites, and pervasive pegmatite veins and dykes of Malari leucogranite to the base of the STD Fault [47]. It crosses the MCT (8 km thick) near Helang, a small village about 12 km downstream from Joshimath, and suddenly, the gradient of the river decreases as it enters the carbonate formations of LHS rocks. The Yamuna originates near the Bandar Poonch peak in the Higher Himalaya, where it flows predominantly to the Higher Himalayan Crystallines of the Almora and the Ramgarh groups, having granodioritic to quartz-dioritic composition [33, 117]. The presence of calc-schists and marble with sulphide mineralization has been reported in the upstream area of Hanuman Chatti [21]. In the downstream, the river drains in the southwest direction, flowing through various litho-units in the outer and inner belts of the Lesser Himalayan [117]. The Tons River is the major tributary of the Yamuna in the Himalaya, which drains the western part of the Yamuna catchment.

It originates in the glacier beyond Har-ki-dun and drains through crystallines and sedimentaries in its upstream and carbonates in the downstream reaches before joining the Yamuna at Kalsi, near Dehradun [21].

Climatic condition

The study area, Alaknanda, Bhagirathi, Yamuna, and Tons rivers (headwater) are situated in the Himalayan region of Uttarakhand State. The Alaknanda and Bhagirathi rivers confluence at Devprayag, where the Ganga river adopts its formal name. The Alaknanda and Bhagirathi river basins occupy an area of about 19.6×10^3 km^2 up to Rishikesh, where the Ganga River enters the plain [17]. The Upper Ganga and Yamuna rivers and tributaries mainly depend on glacier melt and precipitation. The climate of the study area varies from alpine to subtropical. Precipitation is generally received through monsoon rainfall from June to September, and maximum snowfall occurs in December, January, and February. The average annual rainfall in the UGRS and UYRS varies between 1000 and 2500 mm [104]. The amount of rainfall is higher in the upper reaches than in the plains for both the valleys [99]. The annual temperature varies from 0 to 30 °C for the UGRS and UYRS [99].

Methodology

The total water samples (n = 34) were collected from the entire stretches of the UGRS and UYRS (Bhagirathi, Alaknanda, Ganga, Yamuna, and Tons) from the higher Himalaya up to the foothills (Fig. 1, Tables 1, and 2) followed by earlier set international protocols [21, 23, 111, 113] during the COVID-19 lockdown (May and June 2020). The sampling was done from the flowing river water near the bank of the river using a mug or bucket. After rinsing it twice with the sample water, the bottles (High-Density Polyethylene (HDPE) were filled to the top to avoid any headspace. After that, the bottle mouth was sealed with teflon tape. The samples were filtered onsite with a 0.22 µm nylon membrane filter in the field (Millipore®). and stored in bottles for analysis at 4–5 °C. The samples were transported to the Wadia Institute of Himalayan Geology (WIHG) for laboratory measurements and stored in bottles for analysis at 4–5 °C. Field photographs of some of the sample collection sites from the study area are given in (Fig. 2).

The in-situ measurement of physical parameters, namely pH, TDS (mg/l), and EC (µS/cm), were carried out as per the method described by [21, 111, 113] using multi-parameter electrodes and probes (Hach®) with an average precision of ± 0.01 for EC and TDS, ± 0.05 for pH (Table S1 and S2 in the supplementary material). Bicarbonate (HCO_3^-) was analyzed on pH based auto-titrator (Metrohm®).

The major ions (Cl^-, F^-, SO_4^{2-}, NO_3^-, Na^+, K^+, Mg^{2+}, Ca^{2+}) were measured using Ion Chromatography (Dionex series ICS-5000). Primary standards (Dionex, seven anion standard-II, product no. 057590, and six cation-II standard product no. 046070) traceable to the National Institute of Standard Technology (NIST) were measured for calibration of ICS-5000 before the sample analysis followed the standard protocols [111–113]. Normalized Ions Charge Balance (NICB) is presented in Tables S1 and S2 (supplementary material). The data quality is checked by NICB within 5% [22, 111]. The trace elements and dissolved silica concentration were measured in unacidified filtered water samples using a Quadrupole Inductively Coupled Plasma Mass Spectrometer (ICP-MS). In water samples, measurement reproducibility was better than (± 5%) for trace elements dissolved in silica and major ions.

Stable isotopes of oxygen and hydrogen ($\delta^{18}O$ and δD) were measured in the Laser Water Isotope Analyzer (LWIA, Picarro L2140-*i* wavelength-scanned cavity ring-down spectroscopy from Picarro Inc., CA, USA). An aliquot of an unacidified filtered water sample (a 0.22 micron-nylon membrane filter, Millipore®) was filled in 2 ml glass vials and sealed with rubber caps. The vials with the sample were placed in a tray of a PAL auto-sampler connected to the Picarro L2140-*i*. The (2 µl) samples were injected six times into the vaporization module of the analyzer by an auto-sampler at 110°C before being sent into the laser cavity with ultra-pure nitrogen (99.999%) as the carrier gas. The primary standards of (GISP and VSMOW-2) provided by the Atomic Energy Agency (IAEA) were analyzed for the calibration of (LWIA). The reproducibility of measurements was 0.09‰ for $\delta^{18}O$ and 0.5 ‰ for δD.

The Principal component analysis (PCA) is performed in the data sets for data transforming where the structure and the matrix of the data are often exposed once the boundaries of the PCA technique and detection of the scores-scores illustrations. PCA is a technique of Even though a statistical approach will process a collection of figures, whether analytically expressive or not, following this procedure, the new axes, termed principal components (PCs: F1, F2, F3, etc., using the scree plot), are selected based on a linear model Eq. (1).

$$F_{jk} = a_{j1}k_2 + \cdots + a_{jn}k_n \tag{1}$$

where F_{jk} = PC value is j for object k (the score for object j on component k), a_{j1} = the loading of element one on component j, x_{k1} = the length of the score for a variable one on item k, and n is the entire amount of variables observed.

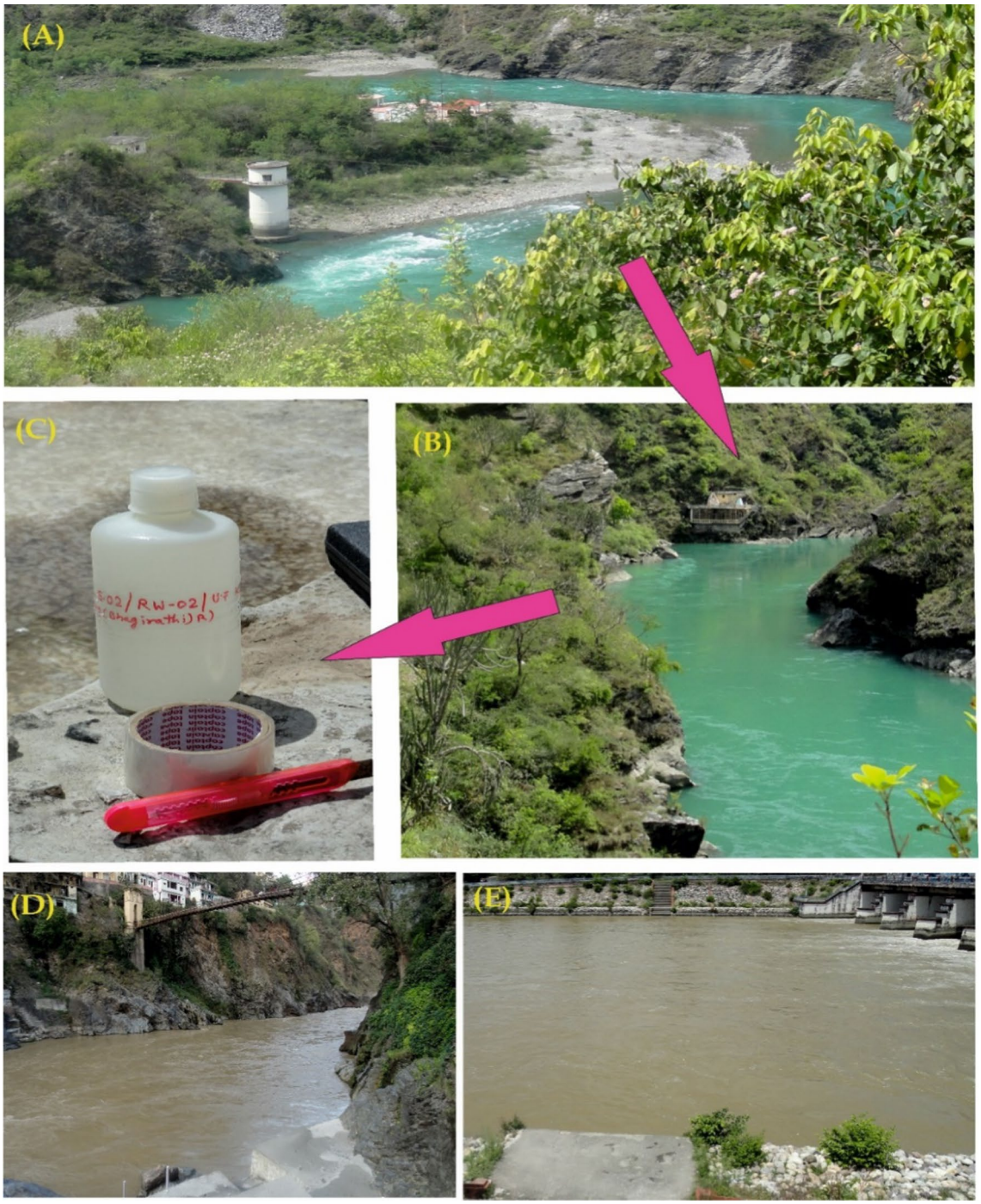

Fig. 2 Field photographs of some sample collection sites from the study area. **A**, **B** Bhagirathi River at Jakholi (BS-1). **C** Sample collected in High-density Poly Ethylene (HDPE) bottle. **D** Alaknanda at Devprayag (AS-2). **E** Ganga at Har Ki Pauri, Haridwar (G-5)

The benefit of this technique is that the variance in the data set is mainly confined to the first few PCs, causing a reduction in the size of the multivariate matrix [126]. The physicochemical parameters (e.g., pH, EC, TDS, HCO_3^-, Na^+, K^+, Mg^{2+}, Ca^{2+}, F^-, Cl^-, NO_3^-, SO_4^{2-}) were taken to evaluate the water pollution index (WPI) values of water samples based on recommended or standard permissible limits as suggested by the Bureau of Indian Standards [12, 119]. WPI is an integrated, weightage-free, and conventional indexing method that converts all input

parameters into a one-value index to assess water quality [9, 42]. To compare the present results with earlier studies [16, 97], these parameters of the same basin were analyzed to estimate their WPI values. In addition, the WPI value of snow and ice from the Dokriani glacier was used to compare the results of different sources and assess the accuracy of this method. First, the pollution load (PL_i) of the ith parameters was calculated by adopting the following equation [42]:

$$PL_i = 1 + \frac{(C_i - S_i)}{S_i} \quad (2)$$

where Ci = observed concentration of i^{th} parameter, Si = standard permissible limit of the i^{th} parameters. In the case of pH, the following equations were used to calculate the PL_i:

$$PL_i = \frac{C_i - 7}{S_{ia} - 7}; \; if \; pH < 7 \quad (3)$$

here, the S_{ia} value is suggested to be the minimum acceptable pH value, i.e., 6.5.

$$PL_i = \frac{C_i - 7}{S_{ib} - 7}; \; If \; pH > 7 \quad (4)$$

where the S_{ib} value would be the maximum acceptable pH value, i.e., 8.5

Finally, the WPI was calculated using the following equation, as suggested by [42]:

$$WPI = \frac{1}{n}\sum_{i=1}^{n} PL_i \quad (5)$$

The relative WPI values were used to scale the water quality. The lower WPI value represents improved water quality, and the reverse is for relatively low water quality.

Results

Geochemical characteristics

A detailed description of the geographical distribution and altitude (m asl) of the collected samples is given in Tables 1 and 2. The major ions, trace elements concentrations, and isotopic compositions of samples are presented in Tables S1 and S2. The UGRS samples were slightly alkaline, with a pH between 7.6 and 8.2, whereas samples from the UYRS were more alkaline, with pH varying from 7.5 to 8.6 during the lockdown Phases 1 and 2. Correlation analysis also supported these results (Tables S5 and S6). The TDS concentration ranged from 47 to 63 mg/L. The dominance order of major ions from the UGRS and UYRS during the lockdown Phases 1 and 2 are as follows: UGRS (Alaknanda, Bhagirathi, and Ganga up to Haridwar)- HCO_3 (45%) > Ca (28%) > SO_4 (10.8%) > Mg (9.19%) > Na (3.67%) > K (1.66%) > Cl (0.96%) > NO_3 (0.43%) > F (0.17%), and UYRS (Yamuna, Tons up to Dakpathar, Vikas Nagar)- HCO_3 (54.1%) > Ca (22.1%) > Mg (8.3%) > SO_4 (6.5%) > Na (5.0%) > Cl (1.7%) > K (1.5%) > NO_3 (0.45%) > F (0.11%). The major ions data were plotted in a Piper diagram (Fig. 3), in which the cations and anions were shown in the bottom left and right triangles, respectively, and further presented in the central diamond to demonstrate the geochemical facies [86]. Most of the samples in the cation triangle were highlighted in the left corner, where Ca^{2+} concentrations were higher (28% for UGRS and 22.2% for UYRS, respectively). In contrast, major anions samples on the right side of the triangle showed elevated concentrations of HCO_3 (45% in the UGRS and 54% in the UYRS, respectively). The geochemical facies of both the UGRS and UYRS were characterized by Ca (25%)-Mg (9%)-HCO_3 (49%) type. The NO_3^- concentration was varied in the UGRS, with a maximum in Alaknanda (~23 µM) followed by Bhagirathi rivers (~20 on average). This concentration is lesser in the UYRS found near Kalsi before its confluence with the Tons River.

The concentrations of measured trace elements (in ppb), namely barium (Ba), strontium (Sr), lithium (Li), lead (Pb), nickel (Ni), molybdenum (Mo), copper (Cu), and cobalt (Co) are presented in Table S1 and S2. The present study observed no health hazard-causing element exceeding their permissible upper limit [12, 119]. In addition, the lowest concentrations of trace elements were observed in the UGRS and UYRS during the lockdown.

Gibbs plot and mixing models

Gibbs plot characterizes the controlling mechanisms in the riverine system, which explain the three end-members, i.e., precipitation, rock weathering, and role of evaporation from bottom to top based on the rations of $[Na^+/(Na^+ + Ca^{2+})$ and $Cl^-/(Cl^- + HCO_3)]$ (Fig. 4) [36]. The samples with low TDS and a high ratio of $[Na^+/(Na^+ + Ca^{2+})$ and $Cl^-/(Cl^- + HCO_3^-]$ reflect the influence of precipitation. Samples with a medium concentration of TDS along with $Na^+/(Na^+ + Ca^{2+})$ and $Cl^-/(Cl^- + HCO_3)$ ratios of < 0.5 showed the dominance of rock weathering that is presented on the middle left side of the plot. The concentration of TDS ≥ 300 mg/L and the ratio of $Na^+/(Na^+ + Ca^{2+}$ or $Cl^-/(Cl^- + HCO_3)$ up to 1.0 implied evaporation or evapo-crystallization as a dominant source of ions. The mixing model prepared using the current data set (Fig. 5) revealed that different groups of major ions could result in different rock weathering rather than other sources.

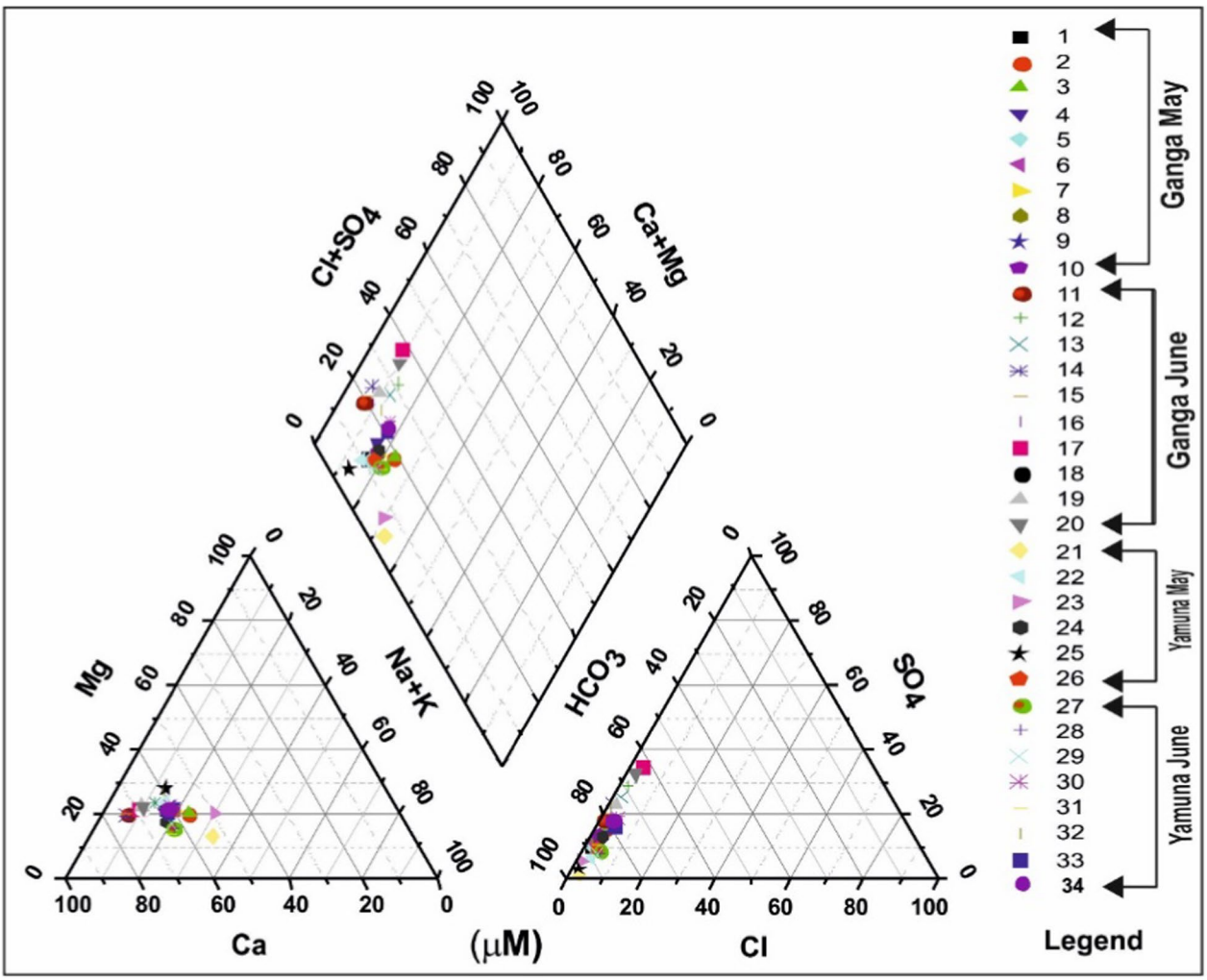

Fig. 3 Piper diagram showing the hydrochemical facies of the Upper Ganga and Yamuna River system

Assessment of water pollution index (WPI)

The WPI index based on the standard permissible limits in surface water is recommended by WHO [119] and BIS [12]. In surface waters, we categorized the WPI into four types to infer the water quality as follows: excellent (WPI < 0.5), good (0.5 < WPI < 0.75), moderate (0.75 < WPI < 1), and highly polluted (WPI > 1). The WPI of water samples collected during the lockdown from the UGRS and UYRS considerably varied from 0.10 to 0.61. The WPI in the studied riverine systems was lower than that reported in a previous study by Chakrapani [16]. Before the confluence with the Yamuna, the Tons River at Khadar had the highest WPI value (0.28–0.32). In contrast, the WPI values for other major river basins (Alaknanda, Bhagirathi, and Ganga) were nearly the same (average ~ 0.14) (Table 3). Notably, the WPI values were the lowest for the snow (~ 0.002) and ice (~ 0.04) of the Dokriani glacier, indicating the freshwater resources feeding the UGRS and UYRS. Furthermore, the change in the percentage of water quality between 2005 and the lockdown period in 2020 was maximum for the Ganga River (Table 3).

4.4. Stable isotopes ($\delta^{18}O$ and δD) systematic

The UGRS and UYRS are mainly fed annually by fresh snow/glacier-melt waters [22, 49, 58, 67, 92, 118] (Fig. 1). We analyzed stable hydrogen (δD) and oxygen ($\delta^{18}O$) isotope ratios of studied riverine systems during the COVID-19 pandemic lockdown Phase 1 and 2. The δD and $\delta^{18}O$ data are presented in Tables S1 and S2, whereas the slope, intercept, and deuterium excess data are shown in Table 4.

Samples from the UGRS had δD values ranging from − 76.16 to − 59.53 with an average of − 65.91 ± 0.1 and $\delta^{18}O$ values from − 10.16 to − 8.55 with an average of − 9.40 ± 0.02; whereas, samples from the UYRS had δD

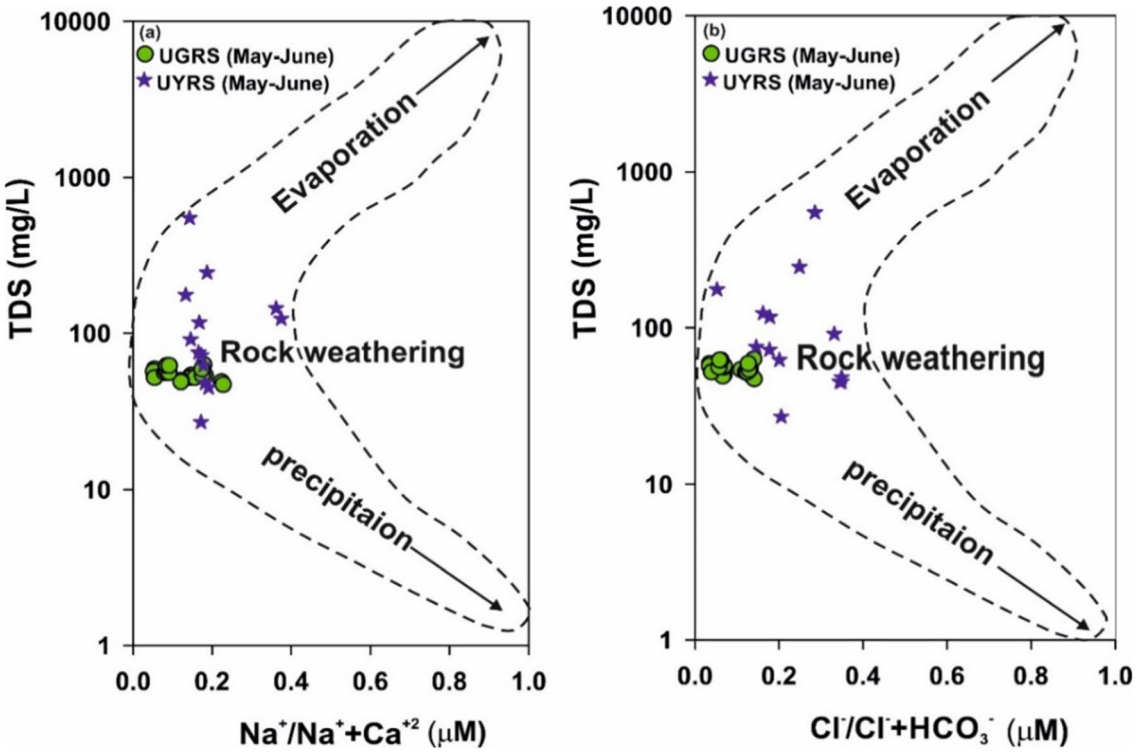

Fig. 4 Gibbs plot showing the Ratios of **a** $(Na^+/(Na^+ + Ca^{2+})$ and **b** $(Cl^-/(Cl^- + HCO_3^-)$ as a function of TDS in the Upper Ganga and Yamuna river system

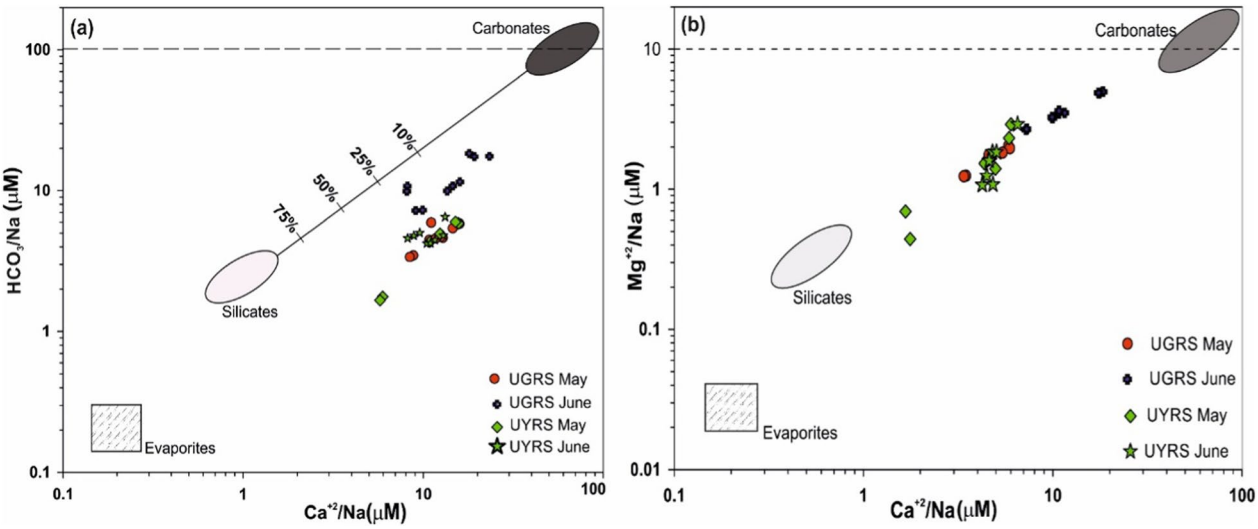

Fig. 5 **a** Mixing diagram of [Ca/Na Vs. HCO3/Na (background data is taken from [71], **b** mixing chart of Ca/Na Vs. Mg/Na (background data obtained from Gaillardet et al. [31]

values varying from − 59.16 to − 43.15 with an average of − 52.9 ± 0.1 and $\delta^{18}0$ values from − 8.76 to − 6.20 with an average of − 7.65 ± 0.02 during the lockdown Phase 1 and 2.

The correlation plot between δD and $\delta^{18}O$ isotope ratios is shown in Fig. 6. The statistical summary, including slope, intercept, p-value, and r^2 of the stable isotope data, along with previously published data, is given in

Table 3 Changes in water quality of the Alaknanda, Bhagirathi, Ganga, and Tons during the Pre-lockdown and lockdown phase

Sample location	Pre-lockdown WPI			During lockdown (Phase- 1 and 2) WPI	% change in WPI	Remarks/relative water quality
	Ramesh and Sarin [92] n = 11	Chakrapani [16] n = 33	Tiwari et al., [112]n = 2	The present study (n = 34)		
Alaknanda	0.10	0.19	–	0.15	21	Improved
Bhagirathi	0.12	0.19	–	0.13	32	Improved
Ganga	0.13	2.0	–	0.14	93	Improved
Tons	–	–	–	0.18	–	Moderately improved
Dokriani glacier			0.03			freshwater

'n' indicates the number of water samples collected in the different river basins.

The Water Pollution Index (WPI) value is shown for the snow and ice of the Dokriani Glacier to check the method's accuracy

Table 4 Slope, Intercept, and deuterium excess calculated based on stable isotopes of oxygen ($\delta^{18}O_{vsmow}$) and hydrogen (δD_{vsmow}) of the upper Ganga and Yamuna River systems and other riverine systems of northwest Himalaya, India

Sites name	No. of sample	Slope	Intercept	P value	r^2	(deuterium excess)		References
						Range	Mean	
Glowal Meteoric Water Line (GMWL)	IAEA network, Worldwide	8.2	10.4	0.001	1	6.1–9.4	8.0 ± 1.9	[96]
Indian Summer Monsoon (ISM) (summer season)	Garhwal region, Northwest Himalaya	7.5 ± 1.5	14.0 ± 0.02	0.001	1	14.9–20.4	18.4 ± 1.1	[118]
Upper Ganga River System (lockdown Phase-1, May 2020)	10	8.70 ± 0.73	15.49 ± 6.59	0.004	0.95	8.46–10.32	9.23 ± 0.63	This study
Upper Ganga River System (lockdown Phase-2, June 2020)	10	6.98 ± 0.39	− 7.8 ± 3.9	0.008	0.97	8.05–10.26	9.32 ± 0.74	This study
Upper Yamuna River System (Lockdown Phase -1, May 2020)	06	5.65 ± 0.74	− 8.7 ± 5.35	0.001	0.94	5.98–10.55	*8.07* ± 1.82	This study
Upper Yamuna River System (Lockdown Phase -2, June 2020)	08	5.81 ± 0.59	− 7.60 ± 4.74	0.002	0.94	8.23–10.94	*9.93* ± 0.95	This study
Dokriani Glacier melt, Garhwal Himalaya (Summer)	23	6.50 ± 1.5	0.03 ± 0.01	0.001	0.94	2.7–21.5	14.6 ± 3.9	[118]
[b] Yamuna River System (postmonsoon)	14	7.71 ± 0.27	7.1 ± 2.3	< 0.002	0.98	5.3–12.8	9.6 ± 2.2	[21]
[b]Yamuna River System (Summer)	28	5.61 ± 0.26	− 9.5 ± 2.1	< 0.002	0.92	5.2–17.3	9.9 ± 3.1	[21]
[b]Yamuna River System (Winter)	31	6.34 ± 0.24	− 1.8 ± 2.1	< 0.002	0.98	7.7–16.2	12.7 ± 2.0	[21]
[c]Upper Ganga River System (Summer)	23	7.45 ± 0.23	− 8.0 ± 2.0	< 0.002	0.98	6.2–21.0	13.7 ± 3.1	[92]

Table 4. The Global Meteoric Water Line (GMWL) [96] and Indian Summer Monsoon Line (ISML) [118] are also plotted for comparison with their best-fit lines (Fig. 6 and Table 4).

Isotopic values in the UGRS were nearly close (slope:7.45 ± 0.23, intercept: − 8.15 ± 2.0) to the observations reported by Ramesh and Sarin [92]. Each tributary/stream of the UGRS and UYRS reflects a distinct isotopic signal due to changes in elevations in its catchment [49]. The samples collected during the lockdown Phase 1 and 2 displayed the maximum contribution of meltwater in the UGRS and UYRS.

The Deuterium excess (*d*-excess) has been practiced for a long time as one of the diagnostic tools to estimate the contribution of water vapor from different sources for a particular location on the globe [48, 67, 84, 118]. d-excess is described by an equation, $d = \delta D - 8^{*}\ \delta^{18}O$ [24], which indicates the deviation in a set of data points from a line with slope 8 in δD vs. $\delta^{18}O$ through a simple regression equation (Table 4). The UGRS and

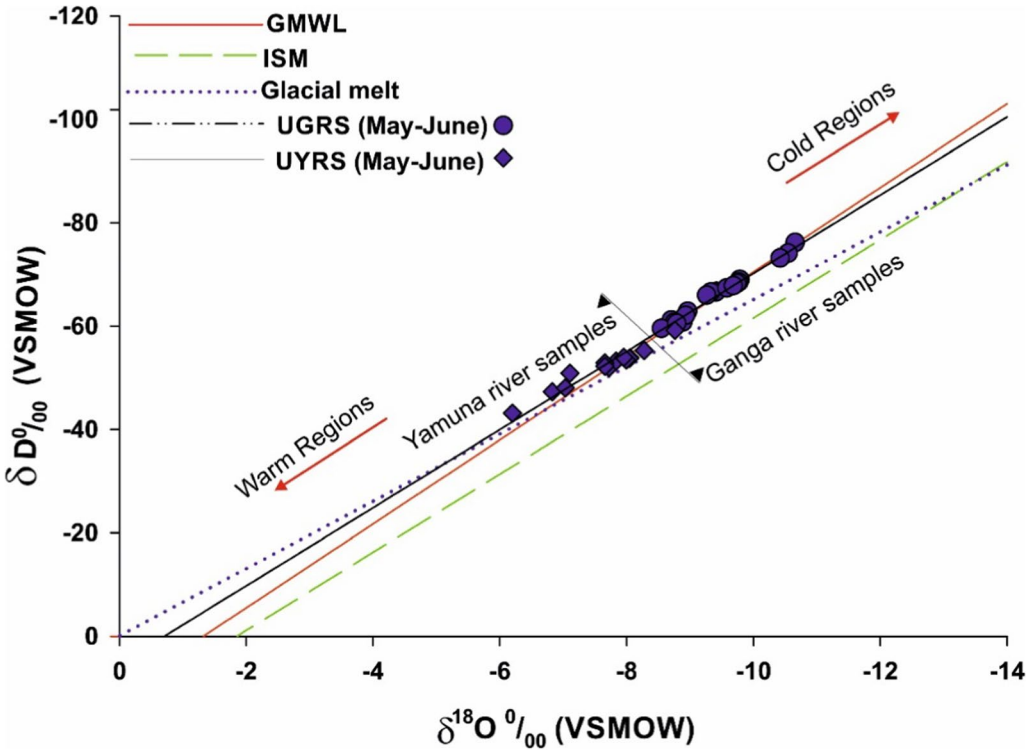

Fig. 6 XY-Plot of stable Isotopic (δD_{vsmow} Vs. $\delta^{18}O_{vsmow}$) systematics of Upper Ganga River and Upper Yamuna River System

UYRS had a d-excess ranging from 6.1 to 9.4 with a mean of 8.0 ± 1.9.

Multivariate metrics

To validate the geochemical analysis, we performed a multivariate analysis that included the PCA in the riverine waters. The PCA is generally calculated in the surface water to evaluate the interrelationship within the available geochemical data set and simplify the complex data [62]. The PCA values of water samples from the UGRS and UYRS, including the Tons river basin, during lockdown Phase 1 and 2 (May and June 2020) are shown in Table 5. From scree plots, the inflection point (eigenvalue > 1) for the UGRS starts at the principal component (PC) sequence number four. In contrast, it occurs at the PC sequence number two for the UYRS (Fig. 7). Any factor with an Eigenvalue > 1 is considered more significant [63]. However, to maintain the differences in inflection points between the UGRS and UYRS, we have extracted three PCs (F1, F2, and F3: Eigenvalues > 1), which are more significant as compared to others and can be utilized to assess the dominant hydro-geochemical processes and their variability (Table 5). Cumulative variance in the UGRS was almost the same in May and June but varied substantially in the UYRS during the same months. A higher eigenvalue indicates higher PC variability, which is evident in the UYRS from May to June. Factor loadings measure the closeness between the input variables and the PC. The first three PCs (F1, F2, F3) account for 83.06% in UGRS, 90.28% in the UYRS of the total variance during May, and 80.80% in the UGRS, and 95.56 in the UYRS of the total variance during June.

In the UGRS (May), the concentrations of pH, F^-, and NO_3^- showed negative loadings for the first principal component (F1), while concentrations of all other variables had positive factor loadings, with higher loadings for EC, TDS, Mg^{2+}, and Ca^{2+}. A higher value of EC is attributed to a strong linkage with major cations like Ca^{2+}, Na^+, and Mg^{2+} [9]. For the second principal component (F2), the concentration of many variables such as pH, EC, TDS, HCO^{3-} and Ca^{2+} had negative loadings, whereas Cl^-, SO_4^{2+}, Na^+, and K^+ showed high positive loadings, contributing more to the water sample. In the third principal component (F3), no higher positive loadings (> 0.8) were found.

In the UGRS (June), the scenario of factor loadings of PCs was quite different compared to May. For F1, the concentration of Na^+ (~ 0.89) had high positive loadings. The concentration of all physical variables and HCO_3^- had negative loadings. Other remaining variables had lower (< 0.5) or moderate positive loadings (0.5 > F1 > 0.8) (Table 5). This indicates that the water quality of the

Table 5 Loadings of experimental variables on principal components analysis (PCA) for the Upper Ganga River System (UGRS) and Upper Yamuna River System (UYRS) in May and June 2020

Factor loadings												
Variables	**UGRS (May)**			**UGRS (June)**			**UYRS (May)**			**UYRS (June)**		
Name of the variable	**F1**	**F2**	**F3**	**F1**	**F2**	**F3**	**F1**	**F2**	**F3**	**F1**	**F2**	**F3**
pH	− 0.257	− 0.230	0.737	− 0.867	− 0.141	0.041	− 0.126	0.491	0.589	0.781	0.321	0.322
Ec (µs/cm)	0.975	− 0.150	0.093	− 0.610	0.649	− 0.275	0.562	0.775	0.254	0.988	− 0.102	0.014
TDS (mg/L)	0.975	− 0.150	0.093	− 0.610	0.649	− 0.275	0.562	0.775	0.254	0.988	− 0.102	0.014
Temp (°C)	0.700	0.115	0.292	− 0.073	0.694	− 0.245	0.433	0.775	− 0.456	0.786	0.102	0.572
HCO_3 (µM)	0.684	− 0.095	− 0.080	− 0.198	0.103	0.809	0.953	− 0.136	0.264	0.971	− 0.072	− 0.166
F (µM)	− 0.722	0.253	0.493	0.343	− 0.691	0.062	− 0.696	0.215	0.287	− 0.791	− 0.223	0.432
Cl (µM)	0.234	0.953	− 0.052	0.784	0.481	− 0.202	0.709	− 0.517	− 0.179	− 0.021	0.983	− 0.137
NO_3 (µM)	− 0.036	0.293	0.765	0.569	− 0.554	0.117	− 0.097	0.700	− 0.685	− 0.479	0.859	0.096
SO_4 (µM)	0.269	0.945	0.077	0.707	0.682	− 0.061	0.664	− 0.363	− 0.584	0.985	− 0.075	0.061
Na (µM)	0.197	0.962	− 0.063	0.899	0.412	0.012	0.235	− 0.243	0.932	0.907	0.370	− 0.090
K (µM)	0.061	0.879	− 0.125	0.606	0.280	0.592	0.914	− 0.183	− 0.206	0.965	− 0.164	− 0.123
Mg (µM)	0.971	0.000	0.142	0.034	0.776	0.559	0.970	0.074	0.216	0.990	0.013	0.010
Ca (µM)	0.896	− 0.345	0.129	− 0.796	0.167	0.546	0.986	− 0.039	0.146	0.985	0.080	− 0.052
Eigenvalue	5.365	3.888	1.545	4.904	3.711	1.890	5.983	3.097	2.657	9.650	2.070	0.703
Variability (%)	41.267	29.906	11.888	37.723	28.542	14.538	46.026	23.821	20.435	74.232	15.920	5.406
Cumulative %	41.267	71.173	83.061	37.723	66.265	80.803	46.026	69.847	90.282	74.232	90.152	95.558

riverine system may be attributed to less anthropogenic and industrial waste input in the river basin during the COVID-19 lockdown. For F2, no variables had high positive loadings (> 0.8), while the concentration of some physio-chemical variables such as temperature, TDS, EC, Mg^{2+}, and SO_4^{2-} showed moderate positive loadings. The pH, F-, and NO_3^- concentrations were characterized by negative loadings for F2. The PC (F3) is not significant for assessing concentrations of variables due to low and moderate loadings, except HCO_3^-.

In the UYRS (May), the first three principal components together account for 90.28% and 95.55% of the total variance of the data set. The concentration of variables such as pH, F^-, and NO_3^- had negative loadings similar to the UGRS (May) load for F1. The HCO_3^-, K^+, Mg^{2+}, and Ca^{2+} showed high positive loadings, whereas the concentrations of SO_4^{2-}, Cl^-, F^-, and TDS had moderate positive loadings. For F2, no variables showed high positive loadings. However, most of the physio-chemical variables indicated moderate positive loadings. For F3, concentrations of Na^+ had high positive loadings.

Discussion

Geochemical source identification and implications against water quality improvement

The COVID-19 pandemic enforced partial and total lockdowns worldwide and provided an unprecedented opportunity to test how lockdown has improved the water quality by reducing the contamination in the water resources. The rock-water interactions resulted in the dissolved ionic compositions in the riverine system. Furthermore, the major ions are added from many sources like solid/liquid precipitation, dust/aerosol, and anthropogenic activities. The congruent and incongruent dissolutions of rock weathering dominate the water composition [16, 57]. In contrast to the pre-lockdown period, we observed increased pH (~ 8 on average) in the post-lockdown, showing a general improvement in the water quality of UGRS and UYRS during the lockdown. Relative increases in pH, i.e., a more alkaline nature of the riverine water in a specific time, may result from reduced anthropogenic activities [28, 129]. The water quality of water bodies, including the Ganga, Yamuna, Mandakini, Alaknanda, Bhagirathi, and Gaula, and the Naini and Bhimtal lakes, were examined based on physical parameters such as pH, TDS, Hardness, etc. [74] during Covid-19 lockdown and observed that all improved due to decreased human activity (tourist, religious activities, rafting, and other sports), as well as a decrease in the flow of industrial effluents. The TDS exhibits the lowest concentrations during the lockdown and is equivalent to the glacier melt [112], which suggests the dominance of major cations from natural weathering sources [28]. Similar variation was observed for EC in both river systems. The correlation matrix showed a strong positive relation between EC and TDS at a 0.05 level of significance

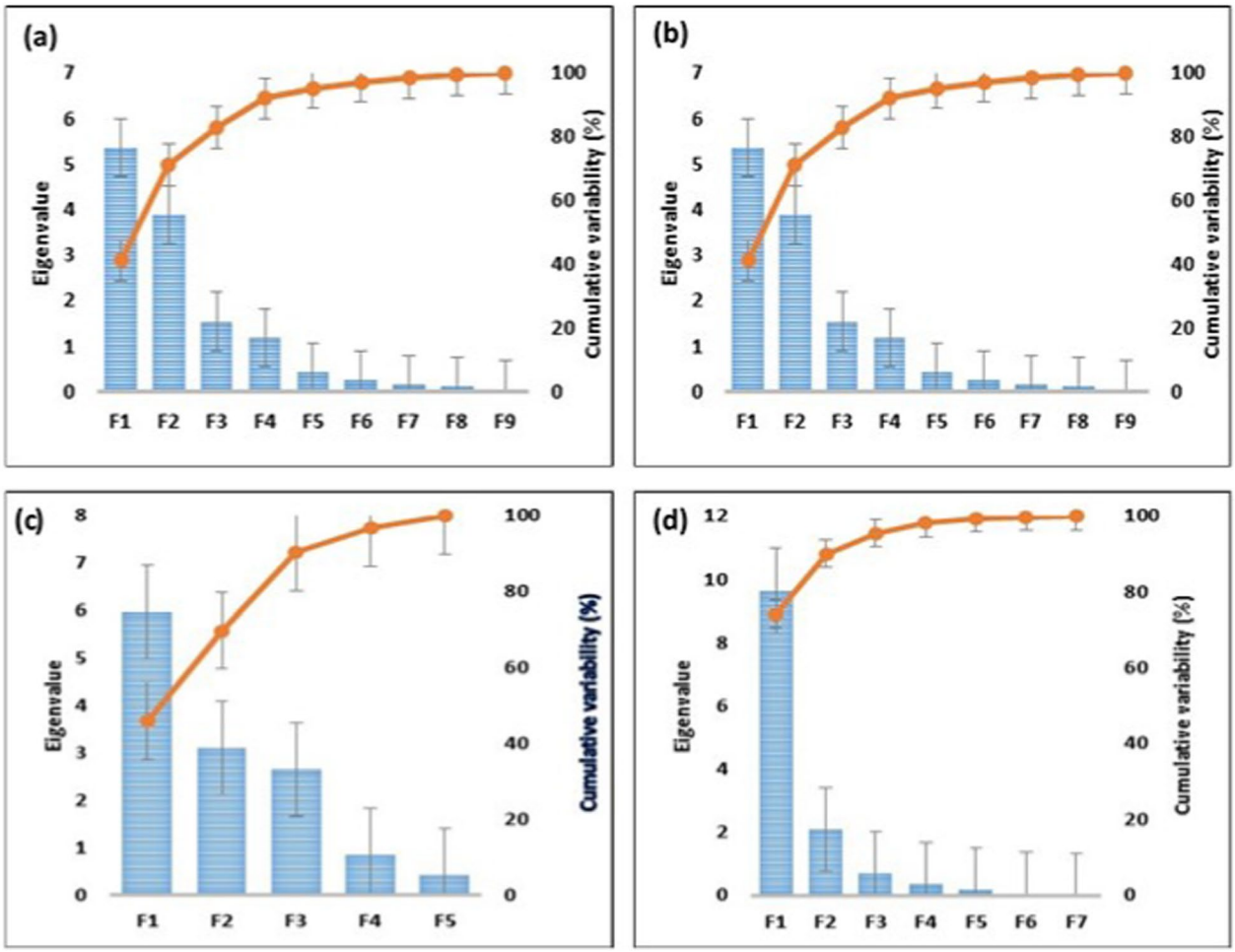

Fig. 7 Scree plots of principal components showing Eigenvalues and cumulative (%) for **a** Upper Ganga River Basin in May; **b** Upper Ganga River Basin in June; **c** Upper Yamuna River Basin in May; **d** Upper Yamuna River Basin in June

(Table S4 and S5 in the supplementary material). EC is directly proportional to the TDS content in the water [15]. No study examined the water quality based on geochemical and isotopic chemistry during the COVID-19 lockdown in this study area. However, based on the physical and other parameters such as dissolved oxygen (DO), biochemical oxygen demand (BOD), total coliforms (TC), and pH, the Central Pollution Control Board of India and the Indian Institute of Technology Roorkee suggested that the water quality of the Ganga and Yamuna River has improved by 40–50% [20]. Khan et al. [53] also reported improved water quality during the COVID-19 lockdown, and industrial wastewater runoff was significantly stopped. A similar study was carried out by Chakraborty et al. [15] in the Damodar River during the COVID-19 lockdown and pre-lockdown phases and found that water samples were substantially contaminated during pre-lockdown. As a result of the halting of the heavy metal industries over three months, 90.90% of water samples were upgraded to good quality, whereas 9.10 percent of samples were moderately polluted.

HCO_3^- was the principal constituent compared to the other ions in both river systems. The sources of various dissolved elements in the riverine system [57] are given in Table S3. Chemical constituents (major and trace elements) in the riverine systems have various sources, including sea salts with chemical, physical, and biological processes carried by atmospheric circulation, which are finally deposited through solid and liquid precipitation. These components undergo different rock weathering, evaporation, and anthropogenic activities [16, 21, 82, 125]. Geochemical facies have described the dominance of calcium, influenced by local sources [51, 102], and HCO_3^- dominated as a major anion, followed by the SO_4^{2-} and Cl^-. SO_4^{2-} and Cl^- had lower concentrations in both riverine systems, indicating a negligible contribution from the anthropogenic sources [122]. The concentration of Na^+ and K^+ is reduced during lockdown,

particularly in the UGRS, compared to the UYRS. However, their concentration is greater than the limiting value in some places, as described by [12]. These major ions showed the presence of urban wastewater, which is increased during lockdown phases near populated areas. Cl^- and NO_3^- enrichments are attributed to anthropogenic activity caused by agricultural waste, rural land uses, and substantial population growth [1, 94].

Six sub-categories are available in the diamond-shaped piper diagram [66]. A detailed description of major ions chemistry of riverine systems along with surface and its controlling factors was described by Gibbs [36]. Few samples from the UYRS fall in the evaporation category, representing the effect of local environmental conditions [87]. In contrast, samples from the UGRS fall in the rock-weathering dominant category (Fig. 4).

The mixing model (Fig. 5) describes the rock-water interaction as silicate weathering that produces mainly sodium, potassium, calcium, magnesium, silica, and bicarbonate in the riverine system. Whereas carbonate weathering produces calcium, magnesium, and bicarbonate, and the dissolution of evaporates, chloride, and nitrate [16, 21, 22, 31, 40, 51, 71, 125]. The traces of SO_4^{2-}, Cl^-, and Na^+ could also be found in the riverine water, obtained from the dissolution of halite, pyrite, gypsum, and anhydrite [83, 87]. Data collected during the lockdown period from the UGRS and UYRS displayed the dominance of silicate weathering with little influence of carbonate weathering.

The WPI exhibits that the water quality started to be contaminated from the beginning of the twentieth century and continued to increase until recent years due to anthropogenic activities, including untreated industrial effluents and urban sewage near the river basins. The WPI values of water samples collected by Sarin et al. [97] are comparable to those of the lockdown phase for the Bhagirathi and the Ganga rivers (Table 3), suggesting that these river systems rejuvenated the water quality to its initial stage, i.e., around 1990. The water of Alaknanda could not be recycled because the WPI value for Alaknanda River was still higher (during lockdown 2020) than that of the water sample taken around 1990. COVID-19 lockdown provides clear information on environmental deterioration triggered by several anthropogenic actions in the past two decades. The lockdown Phases 1 and 2 has significantly reduced pollution due to the temporary closing of the industries and other pollution-deriving agents. However, industrial activities are essential for public livelihood, so the local governing bodies should practice several awareness programs to improve river water quality and the environment.

The isotopic values of both the basins fall on the Global Meteoric water line (GMWL) and the Glacial meltwater line of the Garhwal, northwest Himalaya [118]. However, in this study, the samples collected during the pre-monsoon season showed their trend away from the Indian Summer Monsoon Line (ISML) (Fig. 6), which may result from the westerlies' influence. The stable isotopes of δ18O and δD were depleted in the UGRS, showing that isotopic ratios of δ18O and δD in the basin are more glacierized compared to enriched values of isotopic ratios of δ18O and δD in the UYRS. The Yamuna River (slope: 5.73 ± 0.59 and intercept: $-\ 8.15 \pm 4$) originates from the Yamunotri Glacier near Bandarpunch Peak [90], which is smaller than the Gangotri Glacier. The Bhagirathi River emerges from the second-largest glacier in India, and the Alakananda River contributes to this, which originates from the Satopanth glacier. Hence, the contribution of glacial melt/ fresh snow in the UYRS is also far less than that of the UGRS.

In May and June 2020, we noticed a lower d-excess in the UGRS and UYRS, less comparable to prior research in the same region [21, 92] (Table 4). The observed low d-excess indicated the maximum contribution of glacial melt/fresh snowmelt in the UGRS and UYRS riverine water during the sample collection time.

Statistical substantiation to water quality inferences

In the PCA, the positive loading displays the increased contribution of the variables with the increasing load in the dimensions, while negative loadings show less contribution of the parameters [63]. In our study, the first principal component had the negative factor loading for an anthropogenic element like NO_3 during the lockdown, suggesting its less contribution to UGRS and UYRS river waters [65]. At the same time, positive factor loadings of some cations like HCO_3^-, Ca^{2+}, and Mg^{2+} reflect their strong association with the sources of origin. Positive loadings of the Na^+ indicated that the ionic enrichment factor was dominant due to urban waste [65].

The PC loadings (F1 and F2) relating to the source and water quality are presented in Fig. 8 using the bi-plot for both the UGRS and UYRS during the lockdown. The size of the loadings on the individual PC(s) is represented by a vector drawn from the basis of a set of loadings coordinates, which characterize the sources from which they were derived or related [3, 55]. In the UGRS (May), cluster-1 containing six parameters (temperature, EC, TDS, HCO_3^-, Ca^{2+}, and Mg^{2+}) lies at the rightmost position of the bi-plot (Fig. 8). Their position inferred that they contributed maximum variance and were strongly associated with F1, i.e., their response in the river water sample was strong for May. In the UGRS (June sampling), their relative position from F1 was shifted mostly along with F2, resulting in their relatively weak contribution to the water sample.

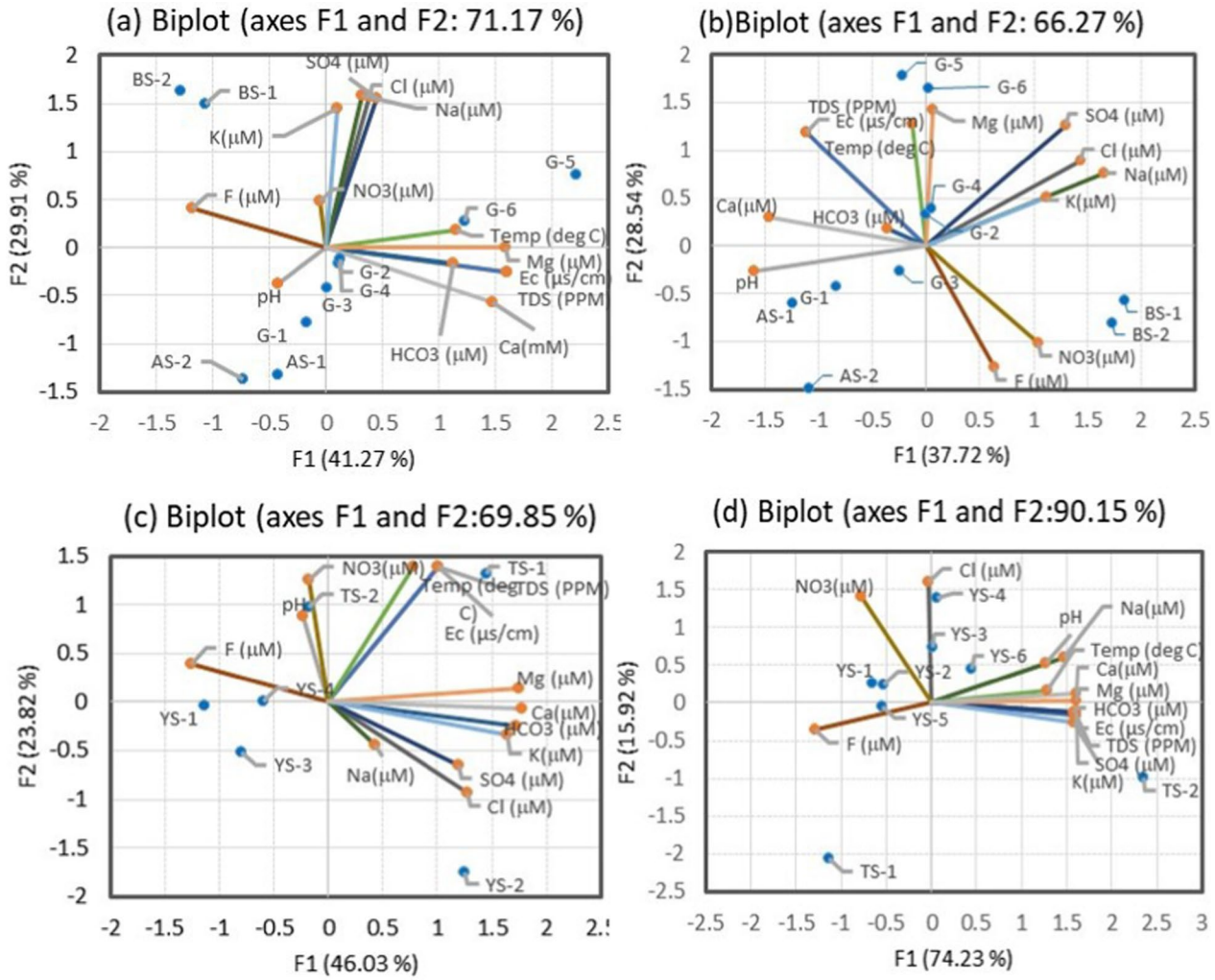

Fig. 8 Bi-plots of PCs 1 and 2 for pattern identification between physicochemical parameters for **a** Upper Ganga River System in May; **b** Upper Ganga River System in June; **c** Upper Yamuna River System in May; **d** Upper Yamuna River System in June 2020

The HCO_3^- position is near the origin of the bi-plot, showing the most negligible contribution in the water sample in May. However, chemically, they are consistent with the typical components of rock minerals. The NO_3^-, which can be derived from organic matter and oxidation of ammonia, largely deviated from cluster 1. Hence, the geological processes consistent with cluster-1 are likely through rock weathering [78, 124]. The UGRS (June) had less variance for F1, contributing weakly to the river basin. A similar contribution was found for Fe^{2+} in June. Cluster-2 containing Na^+, Cl^-, SO_4^{2-}, and K^+ are characterized by positive scores on both F1 and F2. Since two sets of loading vectors (i.e., cluster-1 and 2) are almost 90°, they are uncorrelated from their source of origin. They provide a substantial contribution with F2 in May, which is reduced in June because they are shifted in the middle portion of F1 and F2. Cluster-3 is not well-defined in the bi-plot. pH shifted significantly from the origin in June, showing a significant variance along with F1 compared to the UGRS (May). In the UGRS (June), these clusters no longer remain the same, and their pattern is still somewhat unclear, as it is still hard to separate any trends within each group.

In the UYRS (May), cluster-1 containing Mg^{2+}, Ca^{2+}, K^+, HCO_{3-}, SO_4^{2-}, and Cl^- had positive scores for both F1 and F2. These parameters are strongly associated and positively correlated with their source of origin. They had positive loadings, indicating increased contribution to the river water in June. Cluster-2 containing pH, NO_3^-, TDS, EC, and temperature showed a relatively low correlation with F1, and their clustering is not compact (Fig. 8). In the UYRS (June), the concentration of all variables was inconsistent because their factor scores for F1 and F2 were substantially changed. Only one well-defined cluster with positive scores on F1 and F2 could be found.

The NO_3^- and Fe^{2+} showed a different source of origin, similar to the UGRS (May). In the UYRS (June), factor loading for cluster-1 was almost the same (Fig. 8).

Results from the correlation matrix demonstrate that TDS strongly correlates with EC during the study period (Table S4 and S5 in the supplementary material). Most cations (K^+, Ca^{2+}, Mg^{2+}) strongly correlated with HCO_3, exhibiting their origin from a similar source [59, 88]. In the UGRS, Cl^- showed a good correlation with SO_4^{2-}, Na^+, and K^+, while this relationship was no more substantial for UYRS in June. The NO_3 concentration in both riverine systems had no significant correlation with chemical constituents, reflecting the different sources of its origin. A similar correlation was found with F^- in both river systems. The strongest correlation among the chemical components of river waters was observed in UYRS during June (Table S5). Analysis of the correlation matrix is an effective method to describe the results obtained from chemical analysis [46, 63]. This analysis substantially supported our results derived from physio-chemical analysis.

Overall, multivariate analysis suggests that the source of physio-chemical parameters, such as anthropogenic activity, may be substantially reduced in the river basin in June. These findings illustrate that improvements in water quality during lockdown phases reflect the remarkable environmental impacts of anthropogenic activities. The present study offers a wake-up call to make development pathways environment-friendly.

Conclusions

Our findings draw the following conclusions and recommendations:

- Samples from the UGRS are slightly alkaline, with a pH ranging from 7.6 to 8.2, whereas the UYRS samples are more alkaline, ranging from 7.5 to 8.6.
- The TDS concentration in the UGRS and UYRS was the lowest-ever equivalent to the glacier melt, indicating a little mixing of effluent material from external sources.
- Bicarbonate (HCO3-) is one of the significant elements in both the river basins, followed by other cations and anions, indicating that the geo-genic process was dominant during the lockdown.
- Data obtained during the lockdown period from the Upper Ganga and Yamuna basins clearly show the dominance of silicate weathering with little influence of carbonate weathering.
- The Lockdown phase has significantly reduced the pollution level in water due to the temporary closing of the industries and other pollution-causing agents. Further, we found negligible hazardous trace elements (As, Pb, Ni, etc.) in the UGRS and UYRS.
- PCA evinces the negative factor loading for an anthropogenic element during the lockdown, signifying a reduction in the intake of pollution-causing elements to both UGRS and UYRS.
- The decreased isotope ratios of δ18O and δD suggest a more significant contribution from the glaciated areas in the basin.
- The stable isotopic values (δ18O and δD) are depleted at the headwaters of streams and tributaries and substantially enriched throughout the river basin at lower altitudes.
- The UGRS and UYRS were cleaner during the lockdown than during previous cleaning campaigns, which had cost significant money but never yielded satisfactory results.
- This lockdown shows that we are responsible for preserving nature's purity via sustainable development and resource protection.

Supplementary Information

The online version contains supplementary material available at https://doi.org/10.1186/s12932-024-00092-w.

Additional file 1

Acknowledgements
The authors would like to thank the Director of Wadia Institute of Himalayan Geology (WIHG), Dehradun, for providing all the facilities required to conduct this study during the COVID-19 pandemic-induced lockdown Phase 1 and 2 (May June 2020). We thankful to Mr. Pankaj Kumar Verma (Registrar, WIHG) for taking administrative permission from the state government to conduct fieldwork during the lockdown. This research work was endowed by the Department of Science and Technology (DST), Government of India. This manuscript has the Wadia Institute contribution number WIHG/0178.

Author contributions
Credit authorship contribution statement Sameer K. Tiwari conceptualized the idea, methodology, and sample analysis, conducted fieldwork, and wrote the manuscript. Jairam Singh Yadav performed the PCA analysis. Kalachand Sain made corrections to the manuscript. Santosh K. Rai: Participated in the fieldwork. Aditya Kharya: Participated in the fieldwork, data tabulation, and manuscript formatting. Vinit Kumar participated in the fieldwork and prepared a map. Pratap C. Sethy participated in the fieldwork.

Funding
The authors declare that no funds, grants, or other support were received during the preparation of this manuscript.

Availability of data and materials
No datasets were generated or analysed during the current study.

Declarations

Ethics approval and consent to participate
All authors have read, understood, and complied with the statement on "Ethical responsibilities of Authors" as found in the Instructions for Authors and are aware that with minor exceptions, no changes will be made to authorship

once the paper is submitted. I am free to contact any people involved in the research to seek further clarification and information.

Consent to publication
Not applicable.

Competing interests
The authors declare no competing interests.

Received: 30 April 2024 Accepted: 12 September 2024
Published online: 28 September 2024

References

1. Ako AA, Shimada J, Hosono T, Ichiyanagi K, Nkeng GE, Fantong WY, Roger NN (2011) Evaluation of groundwater quality and its suitability for drinking, domestic, and agricultural uses in the Banana plain (Mbanga, Njombe, Penja) of the Cameroon Volcanic Line. Environ Geochem Health 33(6):559–575
2. Araguás-Araguás L, Froehlich K, Rozanski K (2000) Deuterium and oxygen-18 isotope composition of precipitation and atmospheric moisture. Hydrol Process 14(8):1341–1355. https://doi.org/10.1002/1099-1085(20000615)14:8%3c1341::AID-HYP983%3e3.0.CO;2-Z
3. Ayoko GA, Singh K, Balerea S, Kokot S (2007) Exploratory multivariate modeling and prediction of the physico-chemical properties of surface water and groundwater. J Hydrol 336:115–124. https://doi.org/10.1016/j.jhydrol.2006.12.013
4. Barakat A, El Baghdadi M, Rais J, Aghezzaf B, Slassi M (2016) Assessment of spatial and seasonal water quality variation of Oum Er Rbia river (Morocco) using multivariate statistical techniques. Int Soil Water Conserv Res 4(4):284–292. https://doi.org/10.1016/j.iswcr.2016.11.002
5. BBC news (2020) https://www.bbc.com/news/av/world-asia-india-52290522. Accessed 21 Apr 2020
6. Berner RA, Lasaga AC, Garrels RM (1983) Carbonate-silicate geochemical cycle and its effect on atmospheric carbon dioxide over the past 100 million years. United States. https://doi.org/10.2475/ajs.283.7.641
7. Best J (2019) Anthropogenic stresses on the world's big rivers. Nat Geosci 12(1):7–21. https://doi.org/10.1038/s41561-018-0262-x
8. Bhardwaj V, Singh DS, Singh AK (2010) Water quality of the Chhoti Gandak River using principal component analysis, Ganga Plain, India. J Earth Syst Sci 119:117–127. https://doi.org/10.1007/s12040-010-0007-8
9. Bhat SA, Pandit AK (2014) Surface water quality assessment of Wular Lake, a Ramsar site in Kashmir Himalaya, using discriminant analysis and WQI. J Ecosyst. https://doi.org/10.1155/2014/724728
10. Bickle MJ, Bunbury J, Chapman HJ, Harris NB, Fairchild IJ, Ahmad T (2003) Fluxes of Sr into the headwaters of the Ganges. Geochim Cosmochim Acta 67(14):2567–2584
11. Bindra D, Ravindra K, Chanana N, Mor S (2021) Assessment of on-site sanitation practices and contamination of groundwater in rural areas of Fatehgarh Sahib, Punjab, India. Environ Dev Sustain 23:4594–4613
12. Standard I (2012) Bureau of Indian Standards drinking water specifications. BIS 10500:2012
13. Blum JD, Gazis CA, Jacobson AD, Page Chamberlain C (1998) Carbonate versus silicate weathering in the Raikhot watershed within the High Himalayan crystalline series. Geology 26(5):411–414. https://doi.org/10.1130/0091-7613(1998)026%3c0411:CVSWIT%3e2.3.CO;2
14. Boral S, Sen IS, Ghosal D, Peucker-Ehrenbrink B, Hemingway JD (2019) Stable water isotope modeling reveals spatio-temporal variability of glacier meltwater contributions to Ganges river headwaters. J Hydrol 577:123983. https://doi.org/10.1016/j.jhydrol.2019.123983
15. Chakraborty B, Bera B, Adhikary PP, Bhattacharjee S, Roy S, Saha S, Ghosh A, Sengupta D, Shit PK (2021) Positive effects of COVID-19 lockdown on river water quality: evidence from River Damodar, India. Sci Rep 11(1):1–16. https://doi.org/10.1038/s41598-021-99689-9
16. Chakrapani GJ (2005) Factors controlling variations in river sediment loads. Curr Sci 88:569–575
17. Chakrapani GJ, Saini RK (2009) Temporal and spatial variations in water discharge and sediment load in the Alaknanda and Bhagirathi rivers in Himalaya, India. J Asian Earth Sci 35(6):545–553
18. Chauhan A, Singh RP (2020) Decline in PM2.5 concentrations over major cities around the world associated with COVID-19. Environ Res 187:109634. https://doi.org/10.1016/2Fj.envres.2020.109634
19. CPCB (1986). The environment (protection) act, 1986. https://parivesh.nic.in/writereaddata/ENV/eprotect_act_1986.pdf. Accessed 23 May 1986
20. CPCB (2020), Central pollution control board (CPCB). Water quality. 2020. https://cpcb.nic.in/nwmp-data-2020/. Accessed 5 Nov 2021
21. Dalai TK, Krishnaswami S, Sarin MM (2002) Major ion chemistry in the headwaters of the Yamuna river system: chemical weathering, its temperature dependence and CO2 consumption in the Himalaya. Geochim Cosmochim Acta 66:3397–3416. https://doi.org/10.1016/S0016-7037(02)00937-7
22. Dalai TK, Rengarajan R, Patel PP (2004) Sediment geochemistry of the Yamuna River System in the Himalaya: implications to weathering and transport. Geochem J 38:441–453. https://doi.org/10.2343/geochemj.38.441
23. Dalai TK (2001) Major ions, stable isotopes,^< 87> Sr/^< 86> Sr and Re in the headwaters of the Yamuna: implications to chemical weathering in the Himalaya. Ph. D. Thesis, MS University
24. Dansgaard W (1964) Stable isotopes in precipitation. Tellus 16:436–468. https://doi.org/10.1111/j.2153-3490.1964.tb00181.x
25. Dessert C, Dupré B, François LM, Schott J, Gaillardet J, Chakrapani G, Bajpai S (2001) Erosion of deccan traps determined by river geochemistry: impact on the global climate and the 87Sr/86Sr ratio of seawater. Earth Planet Sci Lett 188(3–4):459–474
26. Down to earth (2020) COVID-19 lockdown: a ventilator for rivers. https://www.downtoearth.org.in/blog/covid-19-lockdownaventilator-for-rivers-70771. Accessed 29 Apr 2020.
27. Dupré B, Gaillardet J, Rousseau D, Allègre CJ (1996) Major and trace elements of river-borne material: the Congo Basin. Geochim Cosmochim Acta 60(8):1301–1321
28. Duttagupta S, Bhanja SN, Dutta A, Sarkar S, Chakraborty M, Ghosh A, Mukherjee A (2021) Impact of COVID-19 lockdown on availability of drinking water in the arsenic-affected ganges river basin. Int J environ Res Public Health 18(6):2832. https://doi.org/10.3390/ijerph18062832
29. Dwivedi S, Mishra S, Tripathi RD (2018) Ganga water pollution: a potential health threat to inhabitants of Ganga basin. Environ Int 117:327–338. https://doi.org/10.1016/j.envint.2018.05.015
30. France-Lanord C, Derry LA (1997) Organic carbon burial forcing of the carbon cycle from Himalayan erosion. Nature 390(6655):65–67
31. Gaillardet J, Dupré B, Louvat P, Allegre CJ (1999) Global silicate weathering and CO2 consumption rates deduced from the chemistry of large rivers. Chem Geol 159:3–30. https://doi.org/10.1016/S0009-2541(99)00031-5
32. Galy A, France-Lanord C (1999) Weathering processes in the Ganges-Brahmaputra basin and the riverine alkalinity budget. Chem Geol 159(1–4):31–60
33. Gansser A (1964) Geology of the Himalayas. Interscience Publishers, London
34. Garg V, Aggarwal SP, Chauhan P (2020) Changes in turbidity along ganga river using sentinel-2 satellite data during lockdown associated with COVID-19. Geomat Nat Hazards Risk 11:1175–1195. https://doi.org/10.1080/19475705.2020.1782482
35. Garrels RM, Mackenzie FT (1972). J: dimentary cycling in relation to the history of the continents and oceans
36. Gibbs RJ (1970) Mechanisms controlling world water chemistry. Science 170:1088–1090. https://doi.org/10.1126/science.170.3962
37. Giri A, Bharti VK, Kalia S, Kumar K, Raj T, Chaurasia OP (2019) Utility of multivariate statistical analysis to identify factors contributing river water quality in two different seasons in cold-arid high-altitude region of Leh-Ladakh, India. Appl Water Sci 9:1–15. https://doi.org/10.1007/s13201-019-0902-3
38. Gremillion P, Wanielista M (2000) Effects of evaporative enrichment on the stable isotope hydrology of a central Florida (USA) river. Hydrol Process 14(8):1465–1484
39. Häder DP, Banaszak AT, Villafañe VE, Narvarte MA, González RA, Helbling EW (2020) Anthropogenic pollution of aquatic ecosystems: emerging problems with global implications. Sci Total Environ 713:136586. https://doi.org/10.1016/j.scitotenv.2020.136586

40. Han G, Liu CQ (2004) Water geochemistry controlled by carbonate dissolution: a study of the river waters draining karst-dominated terrain, Guizhou province, China. Chem Geol 204:1–21. https://doi.org/10.1016/j.chemgeo.2003.09.009
41. Hindustan Times (2020) https://www.hindustantimes.com/india-news/covid-19-lockdown-pollution-in-ganga-declines-as-factories-in-up-uttarakhand-remain-shut/story-ZKGahS4TVfIQqLAOQyHSxM.html. Accessed 28 Apr 2020.
42. Hossain M, Patra PK (2020) Water pollution index—a new integrated approach to rank water quality. Ecol Indic 117:106668. https://doi.org/10.1016/j.ecolind.2020.106668
43. Howladar MF, Al Numanbakth MA, Faruque MO (2018) An application of Water Quality Index (WQI) and multivariate statistics to evaluate the water quality around Maddhapara granite mining industrial area, Dinajpur, Bangladesh. Environ Syst Res 6:1–18. https://doi.org/10.1186/s40068-017-0090-9
44. Immerzeel WW, Van Beek LP, Bierkens MF (2010) Climate change will affect the Asian water towers. Science 328(5984):1382–1385
45. India TV News (2020) https://www.indiatvnews.com/news/india/coronavirus-covid-19-ganga-water-quality-improves-safe-to-drink-607627. Accessed 14 April 2020
46. Iscen CF, Emiroglu Ö, Ilhan S, Arslan N, Yilmaz V, Ahiska S (2008) Application of multivariate statistical techniques in the assessment of surface water quality in Uluabat Lake, Turkey. Environ monit Assess 144:269–276. https://doi.org/10.1007/s10661-007-9989-3
47. Jain AK, Shreshtha M, Seth P, Kanyal L, Carosi R, Montomoli C, Iacca-rino S, Mukherjee PK. (2014) The Higher Himalayan Crystallines, Alaknanda–Dhauli Ganga Valleys, Garhwal Himalaya, India. Eds.) Chiara Montomoli, Rodolfo Carosi, Rick Law, Sandeep Singh, and Santa Man Rai, Geological field trips in the Himalaya, Karakoram and Tibet, Journal of the Virtual Explorer, Electronic Edition, ISSN, 1441–8142
48. Jeelani G, Bhat NA, Shivanna K, Bhat MY (2011) Geochemical characterization of surface water and spring water in SE Kashmir valley, western Himalaya: implications to water–rock interaction. J Earth Syst Sci 120:921–932. https://doi.org/10.1007/s12040-011-0107-0
49. Jeelani G, Kumar US, Kumar B (2013) Variation of δ18O and δD in precipitation and stream waters across the Kashmir Himalaya (India) to distinguish and estimate the seasonal sources of stream flow. J Hydrol 481:157–165. https://doi.org/10.1016/j.jhydrol.2012.12.035
50. Jeelani G, Shah RA, Deshpande RD, Fryar AE, Perrin J, Mukherjee A (2017) Distinguishing and estimating recharge to karst springs in snow and glacier dominated mountainous basins of the western Himalaya, India. J Hydrol 550:239–252. https://doi.org/10.1016/j.jhydrol.2017.05.001
51. Karim A, Veizer J (2000) Weathering processes in the Indus river basin: implications from riverine carbon, sulfur, oxygen, and strontium isotopes. Chem Geol 170:153–177. https://doi.org/10.1016/S0009-2541(99)00246-6
52. Katz BG, Bullen TD (1996) The combined use of 87Sr/86Sr and carbon and water isotopes to study the hydrochemical interaction between groundwater and lakewater in mantled karst. Geochim Cosmochim Acta 60(24):5075–5087
53. Khan I, Shah D, Shah SS (2021) COVID-19 pandemic and its positive impacts on environment: an updated review. Int J Environ Sci Technol 18:521–530. https://doi.org/10.3390/w14071124
54. Khwaja AR, Singh R, Tandon SN (2001) Monitoring of Ganga water and sediments vis-a-vis tannery pollution at Kanpur (India): a case study. Environ Monit Assess 68:19–35
55. Kokot S, Marahusin L, Schweinsberg DP, Jermini M (1994) Characterizing oxidatively damaged cotton fabrics. Part II: A model for the catalytic damage phenomenon using electrogenerated oxygen. Text Res J 64:710–716. https://doi.org/10.1177/2F004051759406401202
56. Kokot S, Grigg M, Panayiotou H, Phuong TD (1998) Data interpretation by some common chemometrics methods. Electroanalysis 10(16):1081–1088
57. Krishnaswami S, Singh SK (2005) Chemical weathering in the river basins of the Himalaya, India. Curr Sci 89:841–849
58. Kumar A, Tiwari SK, Verma A, Gupta AK (2018) Tracing isotopic signatures (δD and δ18O) in precipitation and glacier melt over Chorabari glacier-hydroclimatic inferences for the Upper Ganga Basin (UGB), Garhwal Himalaya. J Hydrol Reg Stud 15:68–89. https://doi.org/10.1016/j.ejrh.2017.11.009
59. Kumar MR, Kumar RV, Sreejani TP, Sravya PVR, Rao GS (2019) Multivariate statistical analysis of water quality of Godavari river at Polavaram for irrigation purposes water. Resour Environ Eng II 115:124. https://doi.org/10.1007/978-981-13-2038-5_12
60. Kumar M, Patel AK, Shah AV, Raval J, Rajpara N, Joshi M, Joshi CG (2020) First proof of the capability of wastewater surveillance for COVID-19 in India through detection of genetic material of SARS-CoV-2. Sci Total Environ 746:141326
61. Kwami CS, Godfrey S, Gavilan H, Lakhanpaul M, Parikh P (2019) Water, sanitation, and hygiene: linkages with stunting in rural Ethiopia. Int J Environ Res Public Health 16(20):3793
62. Lin CY, Abdullah MH, Praveena SM, Yahaya AHB, Musta B (2012) Delineation of temporal variability and governing factors influencing the spatial variability of shallow groundwater chemistry in a tropical sedimentary island. J Hydrol 432:26–42. https://doi.org/10.1016/jjhydrol201202015
63. Ling TY, Soo CL, Liew JJ, Nyanti L, Sim SF, Grinang J (2017) Application of multivariate statistical analysis in evaluation of surface river water quality of a tropical river. J Chem. https://doi.org/10.1155/2017/5737452
64. Liou SM, Lo SL, Wang SH (2004) A generalized water quality index for Taiwan. Environ Monit Assess 96:35–52. https://doi.org/10.1023/B:EMAS000003171583752a1
65. Maji KJ, Chaudhary R (2019) Principal component analysis for water quality assessment of the Ganga River in Uttar Pradesh, India. Water Resour 46:789–806. https://doi.org/10.1134/s0097807819050129
66. Manoj K, Ghosh S, Padhy PK (2013) Characterization and classification of hydrochemistry using multivariate graphical and hydrostatistical techniques. Res J Chem Sci 2231:606
67. Maurya AS, Shah M, Deshpande RD, Bhardwaj RM, Prasad A, Gupta SK (2011) Hydrograph separation and precipitation source identification using stable water isotopes and conductivity: river Ganga at Himalayan foothills. Hydrol Process 25:1521–1530
68. Mishra SP, Sarkar U, Taraphder S, Datta S, Swain D, Saikhom R, Laishram M (2017) Multivariate statistical data analysis-principal component analysis (PCA). Int J Livest Res 7(5):60–78
69. Misra AK (2011) Impact of urbanization on the hydrology of Ganga Basin (India). Water Resour Manag 25:705–719. https://doi.org/10.1007/s11269-010-9722-9
70. Travaglio M, Yu Y, Popovic R, Selley L, Leal NS, Martins LM (2021) Links between air pollution and COVID-19 in England. Environ Pollut 1:2. https://doi.org/10.1016/jenvpol2020115859
71. Moon S, Huh Y, Zaitsev A (2009) Hydrochemistry of the Amur river: weathering in a northern temperate basin. Aquat Geochem 15:497–527. https://doi.org/10.1007/s10498-009-9063-6
72. Muduli PR, Kumar A, Kanuri VV, Mishra DR, Acharya P, Saha R, Sudhakar A (2021) Water quality assessment of the Ganges river during COVID-19 lockdown. Int J Environ Sci Technol 18(6):1645–1652
73. Mukate S, Wagh V, Panaskar D, Jacobs JA, Sawant A (2019) Development of new integrated water quality index (IWQI) model to evaluate the drinking suitability of water. Ecol Indic 101:348–354. https://doi.org/10.1016/jecolind201901034
74. Nandan A, Siddiqui NA, Singh C, Aeri A, Gwenzi G, Ighalo JO, Carvalho Nagliate P, Meili L, Singh P, Chaukura N et al (2021) COVID-19 pandemic in Uttarakhand, India: environmental recovery or degradation? J Environ Chem Eng 9:106595. https://doi.org/10.1016/j.jece.2021.106595
75. Négrel P, Allègre CJ, Dupré B, Lewin E (1993) Erosion sources determined by inversion of major and trace element ratios and strontium isotopic ratios in river water: the Congo Basin case. Earth Planet Sci Lett 120(1–2):59–76
76. New Indian Express. 2020a. Ganga water quality improves, thanks to COVID-19 lockdown across India. https://www.newindianexpresscom/nation/2020/apr/28/ganga-water-quality-improves-thanks-to-covid-19-lockdown-across-india-2136265.html Accessed 28th Apr 2020
77. New Indian Express (2020b). Lockdown effect: Ganga water fit for drinking after decades, say experts. https://www.newindianexpresscom/nation/2020/may/08/lockdown-effect-ganga-water-fit-for-drinking-after-decades-say-experts-2140622.html. Accessed 8 May 2020

78. Olsen RL, Chappell RW, Loftis JC (2012) Water quality sample collection, data treatment and results presentation for principal components analysis–literature review and Illinois river watershed case study. Water Res 46:3110–3122. https://doi.org/10.1016/j.watres.2012.03.028
79. Pal S, Kundu S, Mahato S (2020) Groundwater potential zones for sustainable management plans in a river basin of India and Bangladesh. J Clean Prod 257:120311. https://doi.org/10.1016/jjclepro2020120311
80. Pandey AC, Kaushik K, Parida BR (2022) Google earth engine for large-scale flood mapping using SAR data and impact assessment on agriculture and population of Ganga-Brahmaputra basin. Sustainability 14(7):4210
81. Pandey SK, Singh AK, Hasnain SI (1999) Weathering and geochemical processes controlling solute acquisition in Ganga headwater–Bhagirathi river, Garhwal Himalaya, India. Aquat Geochem 5:357–379
82. Patz JA, Campbell-Lendrum D, Holloway T, Foley JA (2005) Impact of regional climate change on human health. Nat 438:310–317. https://doi.org/10.1038/nature04188
83. Paudyal R, Kang S, Sharma CM, Tripathee L, Huang J, Rupakheti D, Sillanpää M (2016) Major ions and trace elements of two selected rivers near Everest region, southern Himalayas, Nepal. Environ Earth Sci 75:46. https://doi.org/10.1007/s12665-015-4811-y
84. Peng H, Mayer B, Harris S, Krouse HR (2004) A 10-yr record of stable isotope ratios of hydrogen and oxygen in precipitation at Calgary, Alberta, Canada. Tellus B Chem Phys Meteorol 56:147–159. https://doi.org/10.3402/tellusbv56i216410
85. Pesce SF, Wunderlin DA (2000) Use of water quality indices to verify the impact of Córdoba city (Argentina) on Suquıa river. Water Res 34:2915–2926. https://doi.org/10.1016/S0043-1354(00)00036-1
86. Piper AM (1944) A graphic procedure in the geochemical interpretation of water-analyses Eos, Transactions American. Geophys Union 25:914–928. https://doi.org/10.1029/TR025i006p00914
87. Qaisar FUR, Zhang F, Pant RR, Wang G, Khan S, Zeng C (2018) Spatial variation, source identification, and quality assessment of surface water geochemical composition in the Indus River Basin, Pakistan. Environ Sci Pollut Res 25:12749–12763. https://doi.org/10.1007/s11356-018-1519-z
88. Qu W, Kelderman P (2001) Heavy metal contents in the Delft canal sediments and suspended solids of the River Rhine: multivariate analysis for source tracing. Chemosphere 45:919–925. https://doi.org/10.1016/s0045-6535(01)00101-1
89. Quade J, Roe L, DeCelles PG, Ojha TP (1997) The late Neogene 87Sr/86Sr record of lowland Himalayan rivers. Science 276(5320):1828–1831
90. Rai RK, Upadhyay A, Ojha CSP, Singh VP (2011) The Yamuna river basin: water resources and environment, vol 66. Springer Science Business Media, Berlin
91. Rajbhandari B, Phuyal N, Shrestha B, Thapa M (2020) Air medical evacuation of Nepalese citizen during epidemic of COVID-19 from Wuhan to Nepal. J Nepal Med Assoc 58:222. https://doi.org/10.31729/jnma4857
92. Ramesh R, Sarin MM (1992) Stable isotope study of the Ganga (Ganges) river system. J Hydrol 139:49–62. https://doi.org/10.1016/0022-1694(92)90194-Z
93. Rani N, Sinha RK, Prasad K, Kedia DK (2011) Assessment of temporal variation in water quality of some important rivers in middle Gangetic plains, India. Environ Monit Assess 174:401–415
94. Ray C, Schock SC (1996) Comparability of large-scale studies of agricultural chemical contamination of rural private wells ground water. Monit Remed 16(2):92–102
95. Ray Y, Srivastava P (2010) Widespread aggradation in the mountainous catchment of the Alaknanda-ganga river system: timescales and implications to Hinterland–foreland relationships. Quat Sci Rev 29(17–18):2238–2260
96. Rozanski K, Araguás-Araguás L, Gonfiantini R (1993) Isotopic patterns in modern global precipitation. Clim Chang Cont Isot Rec. 78:1–36. https://doi.org/10.1029/GM078p0001
97. Sarin MM, Krishnaswami S, Trivedi JR, Sharma KK (1992) Major ion chemistry of the Ganga source waters: weathering in the high altitude Himalaya Proc Indian Acad Sci-Earth Planet. Sci 101:89–98. https://doi.org/10.1007/BF02839175
98. Sarin MM, Krishnaswami S, Dilli K, Somayajulu BLK, Moore WS (1989) Major ion chemistry of the Ganga-Brahmaputra river system: weathering processes and fluxes to the Bay of Bengal. Geochim Cosmochim Acta 53(5):997–1009
99. Sati VP (2008) Natural resources management and sustainable development in Pindar Valley, Himalayas. Bishen Singh Mahendra Pal Singh
100. Schwarzenbach RP, Egli T, Hofstetter TB, Von Gunten U, Wehrli B (2010) Global water pollution and human health. Annu Rev Environ Resour 35(1):109–136
101. Searle MP, Cottle JM, Streule MJ, Waters DJ (2009) Crustal melt granites and migmatites along the Himalaya: melt source, segregation, transport and granite emplacement mechanisms. Earth Environ Sci Trans R Soc Edinb 100(1–2):219–233
102. Selemani JR, Zhang J, Muzuka AN, Njau KN, Zhang G, Maggid A, Mzuza MK, Jin J, Pradhan S (2017) Seasonal water chemistry variability in the Pangani River basin, Tanzania. Environ Sci Pollut Res 24:26092–26110. https://doi.org/10.1007/s11356-017-0221-x
103. Sen IS, Nizam S, Ansari A, Bowes M, Choudhary B, Glendell M, Sinha R (2023) Geochemical evolution of dissolved trace elements in space and time in the Ramganga River, India. Environ Monit Assess 195(10):1150
104. Sharma A, Sharma D, Panda SK (2022) Assessment of spatiotemporal trend of precipitation indices and meteorological drought characteristics in the Mahi River basin, India. J Hydrol 605:127314
105. Singh AK, Hasnain SI (1998) Major ion chemistry and weathering control in a high altitude basin: Alaknanda river, Garhwal Himalaya, India. Hydrol Sci J 43(6):825–843
106. Singh S (2018) Alakhnanda-Bhagirathi river system. In: Singh DS (ed) The Indian rivers: scientific and socio-economic aspects. Springer, Singapore, pp 105–114. https://doi.org/10.1007/978-981-10-2984-4_8
107. Singh VB, Ramanathan AL, Pottakkal JG, Kumar M (2014) Seasonal variation of the solute and suspended sediment load in Gangotri glacier meltwater, central Himalaya, India. J Asian Earth Sci 79:224–234
108. Stallard RF, Edmond JM (1983) Geochemistry of the Amazon: 2. The influence of geology and weathering environment on the dissolved load. J Geophys Res Oceans 88(C14):9671–9688
109. Times of India (2020a) https://timesofindia.indiatimes.com/india/how-lockdown-has-been-a-gift-for-river-ganga/articleshow/75569852.cms. Accessed 6 May 2020
110. Times of India (2020b). https://timesofindia.indiatimes.com/india/lockdown-improves-water-quality-of-ganga-yamuna/articleshow/75456921.cms. Accessed 29 Apr 2020
111. Tiwari SK, Gupta AK, Asthana AK (2020) Evaluating CO2 flux and recharge source in geothermal springs, Garhwal Himalaya, India: stable isotope systematics and geochemical proxies. Environ Sci Pollut Res 13:1–8. https://doi.org/10.1007/s11356-020-07922-1
112. Tiwari SK, Gupta AK, Verma A, Bhambri R, Sundriyal S, Yadav JS (2018) Hydrochemistry of meltwater from Dokriani Glacier during early and draining late ablation season, West Central Himalaya. Him Geol 3:121–132
113. Tiwari SK, Rai SK, Bartarya SK, Gupta AK, Negi M (2016) Stable isotopes (δ13CDIC, δD, δ18O) and geochemical characteristics of geothermal springs of Ladakh and Himachal (India): evidence for CO_2 discharge in northwest Himalaya. Geothermics 64:314–330. https://doi.org/10.1016/jgeothermics201606012
114. Tripathi M, Singal SK (2019) Use of principal component analysis for parameter selection for development of a novel water quality index: a case study of river Ganga India. Ecolg Indicat. 96:430–436. https://doi.org/10.1016/jecolind201809025
115. Trombadore O, Nandi I, Shah K (2020) Effective data convergence, mapping, and pollution categorization of ghats at Ganga River Front in Varanasi. Environ Sci Pollut Res 1:27. https://doi.org/10.1007/s11356-019-06526-8
116. Tsegaye T, Sheppard D, Islam KR, Tadesse W, Atalay A, Marzen L (2006) Development of chemical index as a measure of in-stream water quality in response to land-use and land cover changes. Water Air Soil Pollut 174:161–179. https://doi.org/10.1007/s11270-006-9090-5
117. Valdiya KS (1980) The two intracrustal boundary thrusts of the Himalaya. Tectonophysics 66:323–348. https://doi.org/10.1016/0040-1951(80)90248-6
118. Verma A, Kumar A, Gupta AK, Tiwari SK, Bhambri R, Naithani S (2018) Hydroclimatic significance of stable isotopes in precipitation from glaciers of Garhwal Himalaya, Upper Ganga Basin (UGB), India. Hydrol Process 32:1874–1893. https://doi.org/10.1002/hyp13128
119. WHO (2011) Guidelines for drinking-water quality, 4th edn. WHO, Geneva

120. WHO (2020). World Health Organization, Coronavirus disease 2019 (COVID-19) Situation Report-163. https://www.who.int/docs/default-source/coronaviruse/situation-reports/20200701-covid-19-sitrep-163.pdf. Accessed 01 July 2020
121. Wissler Gerdes EO, Zhu Y, Tchkonia T, Kirkland JL (2020) Discovery, development, and future application of senolytics: theories and predictions. FEBS J 287:2418–2427
122. Xiao J, Jin ZD, Ding H (2012) Geochemistry and solute sources of surface waters of the Tarim River Basin in the extreme arid region, NW Tibetan Plateau. J Asia Earth Sci. 54:162–173. https://doi.org/10.1016/jjseaes201204009
123. Yadav SK, Chakrapani GJ (2011) Geochemistry, dissolved elemental flux rates, and dissolution kinetics of lithologies of Alaknanda and Bhagirathi rivers in Himalayas, India. Environ Earth Sci 62:593–610
124. Zhang BY, Zhang JH, Sun GL (2015) Deformation and shear strength of rockfill materials composed of soft siltstones subjected to stress, cyclical drying/wetting and temperature variations. Eng Geol 190:87–97. https://doi.org/10.1016/j.enggeo.2015.03.006
125. Zhang SR, Lu XX, Higgitt DL, Chen CT, Sun HG, Han JT (2007) Water chemistry of the Zhujiang (Pearl river): natural processes and anthropogenic influences. J Geophys Res Earth Surf. https://doi.org/10.1029/2006JF000493
126. Zhao J, Fu G, Lei K, Li Y (2011) Multivariate analysis of surface water quality in the three Gorges area of China and implications for water management. J Environ Sci 23:1460–1471. https://doi.org/10.1016/S1001-0742(10)60599-2
127. Zhao S, Hu H, Tian F, Tie Q, Wang L, Liu Y, Shi C (2017) Divergence of stable isotopes in tap water across China. Sci Rep 7(1):43653
128. Zhu H, Wei L, Niu P (2020) The novel coronavirus outbreak in Wuhan, China. Glob Health Res Policy 5(1):1–3. https://doi.org/10.1186/s41256-020-00135-6
129. Zouch H, Cabrol L, Chifflet S, Tedetti M, Karray F, Zaghden H, Sayadi S, Quéméneur M (2018) Effect of acidic industrial effluent release on microbial diversity and trace metal dynamics during resuspension of coastal sediment. Front Microbiol 9:3103. https://doi.org/10.3389/fmicb201803103

Publisher's Note